




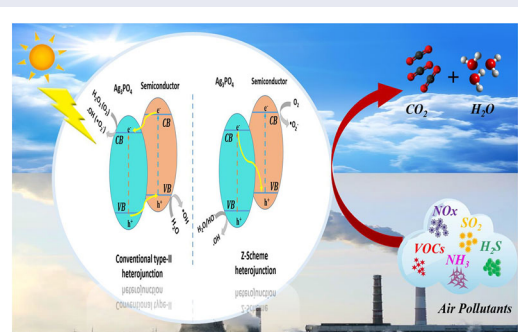
Photocatalytic oxidation of pollutants in gas-phase via Ag_3PO_4 -based semiconductor photocatalysts: Recent progress, new trends, and future perspectives





Y. Naciri^{a,b,*}, A. Hsini^{a,*}, A. Bouziani^c, R. Djellabi^{d,e}, Z. Ajmal^f, M. Laabd^a , J. A. Navío^g, A. Mills^h, C. L. Bianchi^d, H. Li^b, B. Bakiz^a, and A. Albourine^a

^aLaboratoire Matériaux et Environnement LME, Faculté des Sciences, Université Ibn Zohr, Agadir, Morocco; ^bInstitute for Energy Research, School of Chemistry and Chemical Engineering, Jiangsu University, Zhenjiang, P. R. China; ^cChemical Engineering Department, Middle East Technical University, Ankara, Turkey; ^dDepartment of Chemistry, Università degli Studi di Milano, Milano, Italy; ^eResearch Center for Eco-Environmental Sciences, Chinese Academy of Sciences Beijing, China; ^fCollege of Engineering, China Agricultural University, Beijing, P. R. China; ^gInstituto de Ciencia de Materiales de Sevilla, Centro Mixto, Universidad de Sevilla-CSIC, Sevilla, Spain; ^hSchool of Chemistry and Chemical Engineering, Queens University Belfast, Belfast, UK


ABSTRACT

Air pollution has become a significant challenge for both developing and developed nations. Due to its close association with numerous fatal diseases such as cancer, respiratory, heart attack, and brain stroke. Over recent years, heterogeneous semiconductor photocatalysis has emerged as an effective approach to air remediation due to the ease of scale-up, ready application in the field, use of solar light and ready availability of a number of different effective photocatalysts. To date, most work in this area has been conducted using UV-absorbing photocatalysts, such as TiO_2 and ZnO ; However, recent studies have revealed Ag_3PO_4 as an attractive, visible-light-absorbing alternative, with a bandgap of 2.43 eV. In particular, this material has been shown to be an excellent photocatalyst for the removal of many types of pollutants in the gas phase. However, the widespread application of Ag_3PO_4 is restricted due to its tendency to undergo photoanodic corrosion and the poor reducing power of its photogenerated conduction band electrons, which are unable to reduce O_2 to superoxide $\bullet\text{O}_2^-$. These limitations are critically evaluated in this review. In addition, recent studies on the modification of Ag_3PO_4 via combination with the conventional heterojunctions or Z-scheme junctions, as well as the photocatalytic mechanistic pathways for enhanced gas-pollutants removal,



CONTACT Y. Naciri  yassine.naciri@edu.uiz.ac.ma  Laboratoire Matériaux et Environnement LME, Faculté des Sciences, Université Ibn Zohr, Cité Dakhla, Agadir BP 8106, Morocco; J. A. Navío  navio@us.es  Instituto de Ciencia de Materiales de Sevilla, Centro Mixto, Universidad de Sevilla-CSIC, Américo Vespucio 49, Sevilla 41092, Spain.

*These authors contributed equally to this work.

 Supplemental data for this article can be accessed at [publisher's website](#).

are summarized and discussed. Finally, an overview is given on the future developments that are required in order to overcome these challenges and so stimulate further research into this promising field.

KEYWORDS Ag₃PO₄; conventional heterojunctions; gaseous pollutants; photocatalytic oxidation process; Z-scheme junctions

1. Introduction

Rapid population and industrial growth represent the two main underlying causes for environmental pollution, associated with a wide variety of pollutants which enter the natural environment every year (Aarab et al., 2020; Abdellaoui et al., 2021; Ajmal et al., 2018; Ba Mohammed et al., 2020; Essekre et al., 2020; Hsini, Essekre, et al., 2020, Hsini et al., 2021; Qadeer et al., 2020, 2019). Typical indoor air pollutants include volatile organic compounds (VOCs), particulate matter (PM), and inorganic oxides (NO_x and SO_x). According to the world health organization survey, air pollution results in the death of about 7 million people around the globe. 4.3 million people are severely affected by indoor air pollution. It is estimated that one in eight total global deaths is due to conditions associated with poor air quality, and as a result, air pollution is considered by many to represent the biggest environmental health risk (da Costa Filho & Vilar, 2020; Cho, 2017).

In order to reduce the effects of air pollution, most standard air purifying systems use air filters to remove particulate matter and adsorbents (e.g., magnetite, almond shell derived biomass, granular activated carbon) to remove VOCs. However, these technologies do not destroy the pollutants, but rather only transfer them from one phase to another (Ajmal, Usman, et al., 2020; Ajmal, Muhmood, et al., 2020; Benafqir et al., 2020; Hsini, Naciri, Laabd, et al., 2020; Sansotera et al., 2019; Zhao & Yang, 2003). Hence, an urgent current topic for policymakers and scientists is to explore and introduce new cost-effective treatment strategies to overcome the existing air pollution problem.

Heterogeneous semiconductor photocatalysis is regarded as an effective alternative technology for both water and air purification (Ait Ahsaine et al., 2018; Barebita et al., 2020; Bouziani et al., 2020; Erdogan et al., 2019; Naciri, Hsini, Ajmal, Navío, et al., 2020; Ferraa et al., 2021; Shaim et al., 2019). As a result it is often classified into the following two categories, (i) Aqueous phase organic pollutants degradation (Amaterz, Tara, Bouddouch, Taoufyq, Bakiz, Benhachemi, et al., 2020; Amaterz, Tara, Bouddouch, Taoufyq, Bakiz, Lazar, et al., 2020; Deng et al., 2020; Fiorenza et al., 2020;

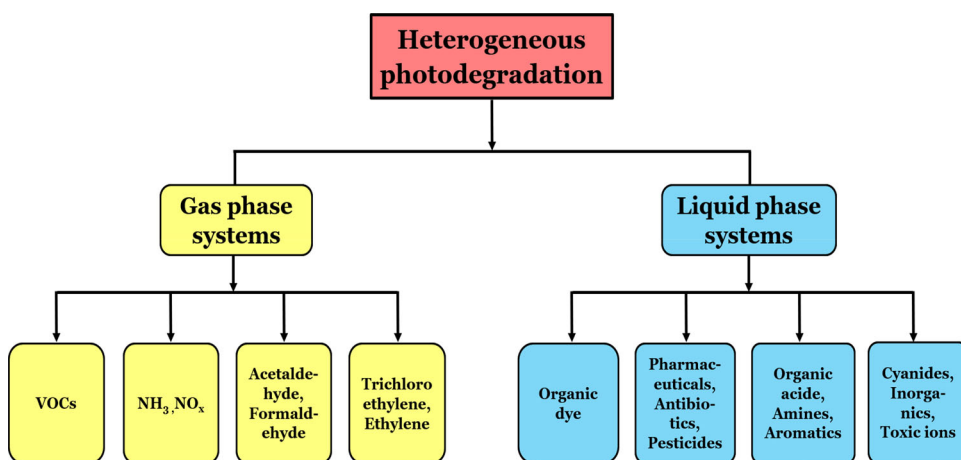


Figure 1. Heterogeneous photocatalytic remediation systems for various pollutants.

Naciri, Hsini, Ajmal, Bouddouch, et al., 2020; Naciri, Chennah, et al., 2019, Naciri, Bouddouch, et al. 2019; Naciri et al., 2018) and (ii) Gaseous phase pollutants removal (Aramendía et al., 2007; Araña et al., 2004; Liao et al., 2017; Reyna-Cavazos et al., 2020), and Figure 1 illustrates a schematic that further sub-divides these areas of application into different types of pollutants.

Semiconductor photocatalysis, SPC, has attracted considerable research interest over the last few decades owing to its great potential to effect the continuous elimination of gaseous pollutants even at low concentrations and at low or room temperature (Aramendía et al., 2007; Araña et al., 2009, 2004; Murcia et al., 2012). SPC, appears most efficient for photocatalysing the complete oxidative mineralization of a wide range of gaseous pollutants (i.e., volatile organic compound, simple and chlorinated hydrocarbons and different nitrogen and sulfur-based oxides-dioxides) by ambient oxygen (Aramendía et al., 2007; Araña et al., 2009, 2004; Murcia et al., 2012; Zhou et al., 2019). Since the first report on the use of SPC for organic destruction (Bickley et al., 1973; Djeghri et al., 1974), the photocatalytic oxidation of gaseous contaminants has been extensively studied, to confirm the validity and attractiveness of the method.

Although many semiconductor photocatalysts have been tested, TiO_2 remains the most popular due to its low cost, high chemical and photochemical stability, low toxicity and generally high activity. However, TiO_2 has one major drawback in wide bandgap (approximately 3.2 eV), which renders only effective under UV illumination. Solar UV represents about 5% of the energy of the whole solar spectrum, while visible light represents 43%. Therefore, the development of visible-light-driven photocatalysts has become a subject of prime importance in the field of SPC for pollutants degradation (Chenchana et al., 2019; Likodimos, 2018; Mazierski et al., 2018; Puga et al., 2020).

Recently, several Ag-based materials, including AgX (X = Cl, Br, I) (Wang et al., 2019; Wen et al., 2020; Xin et al., 2019), Ag₂O (Liang et al., 2019), Ag₂CO₃ (Liu et al., 2018), and Ag₃PO₄ (Martín-Gómez et al., 2020), have been reported as exhibiting high photocatalytic activity even under natural sunlight or visible light illumination and amongst the materials tested, Ag₃PO₄ appears the most promising (Chen et al., 2015, 2013). Other work indicates that the high photocatalytic activity exhibited by Ag₃PO₄ is due to the inductive effect of PO₄³⁻ and the large dispersion of the conduction band, both of which aids electron-hole pairseparation (Chen et al., 2013). Unfortunately, there are some major inherent shortcomings with regard to the use of Ag₃PO₄ in the photodecomposition of gaseous organic contaminates. One shortcoming is the very positive conduction band of Ag₃PO₄ (+0.45 V vs. NHE at pH 0) which makes it unable to effect the reduction of O₂ to superoxide, since $E(\text{O}_2/\bullet\text{O}_2^-) = -0.33 \text{ V vs. NHE}$ (Wood, 1988). As a result, the photogenerated conduction band electrons of Ag₃PO₄ cannot react with O₂, which is a key part of the photocatalytic mineralization process. In addition, in the absence of an effective ambient sacrificial electron acceptor, such as O₂, the photogenerated electrons are able to reduce the Ag(I) in the Ag₃PO₄ itself and so destroy the efficacy of the original photocatalyst due to Ag particle by-product formation. The above two limitations affect significantly the photocatalytic activity and stability and ultimately restricts the potential practical applications of Ag₃PO₄ (Chai et al., 2015; Li et al., 2014, 2015).

As a consequence, it is necessary to introduce ways to improve the photocatalytic activity and stability of Ag₃PO₄ (Chai et al., 2015; Li et al., 2014, 2015). One approach has been to couple Ag₃PO₄ with a more stable semiconductor photocatalyst, thereby forming a heterojunction, and in doing so enhance the stability of Ag₃PO₄ for the reduction/removal of inorganic gas pollutants (Chen et al., 2015; Guo et al., 2013; Huang et al., 2019; Jia et al., 2019; Rao et al., 2020; Rawal et al., 2012).

To the best of our knowledge, this is the first review addressing the reported research progress on the photocatalytic remediation of air using Ag₃PO₄-based semiconductor photocatalytic systems. We start with a general overview of the current control techniques for gas-phase pollutants removal and their limitations. Then, the photocatalytic properties of Ag₃PO₄ and its limitations as a photocatalyst are discussed in detail. The improving photocatalytic activities of Ag₃PO₄ photocatalyst toward gaseous-phase pollutants by constructing conventional heterojunctions or Z-scheme junction photocatalytic systems are then addressed as the main part of this review. Finally, numerous ways are presently proposed for future research to overcome the existing challenges and design the most promising heterojunctions based photocatalyst for air pollution reduction strategy.

2. General overview of the current control techniques for the removal of pollutants in gas-phase

Many physicochemical abatement methods have been used extensively for the effective removal of gaseous pollutants; these methods include, adsorption (Li et al., 2020), absorption (Rodriguez Castillo et al., 2019), condensation (Belaissaoui et al., 2016), botanical purification (Pettit et al., 2019, 2018), catalytic combustion (Fino et al., 2016), photocatalytic oxidation (Kamal et al., 2016), bio-filtration (Malakar et al., 2017), plasma oxidation (Malakar et al., 2017), biodegradation (Malakar et al., 2017), and membrane separation (Malakar et al., 2017). Based on the removal mechanism, we can further classify these abatement techniques into two categories: concentration and recovery techniques (adsorption, absorption, filtration, and condensation) and destructive techniques (catalytic combustion, plasma oxidation, biodegradation, and botanical purification). The destructive gas cleaning techniques are mainly based on the conversion of gas-phase organic contaminants into water vapor, carbon dioxide, and other smaller molecules by-products (Ehn et al., 2014), which usually require a large amount of energy to effect, and inevitably produce some toxic byproducts such as NO_x, O₃, HO• radicals, secondary organic aerosols, etc. (Ehn et al., 2014; Li et al., 2020). In contrast, recovery technologies have often been reported as more efficient and economical gas cleaning strategies (Zhang et al., 2017). Among them, adsorption is recognized as one of the most promising strategies to abate the gas-phase pollutants, which does not produce secondary by-products (Li et al., 2020). In the adsorption process, the storage of gaseous pollutants on the surface of adsorbent material is commonly carried out via a pore-filling mechanism combined with the eventual formation of physical and/or chemical gas-adsorbent bindings (Zhu et al., 2020). Thus, the effectiveness and real applicability of adsorption techniques for gas pollutants abatement are ultimately associated with adsorbent surface properties, such as binding functional groups and a porous, i.e. high surface area, texture (Li et al., 2020). In this regard, a large variety of adsorbents, including carbon-based materials (Azzouz et al., 2018; Zhang et al., 2017), organic polymers (Azzouz et al., 2018; Zhu et al., 2020), aluminosilicates (Swetha et al., 2017; Zhang et al., 2018), resins (Qiu et al., 2018), silica gels (Amonette & Matyáš, 2017; Sui et al., 2017) and metal-organic frameworks (Barea et al., 2014; Xian et al., 2015) have been recently developed to sequester gas-phase contaminants. Amongst these, activated carbon is a popular filter material with excellent gas sequestration ability because of its high surface area, microporous structure, surface chemistry, etc. (Shammy et al., 2016; Suresh & Bandosz, 2018). Nevertheless, the adsorption is a transfer process of pollutants from the gas phase to the solid phase, which requires a posttreatment to oxidatively mineralize

the adsorbed pollutants (Jo & Yang, 2009; Thevenet et al., 2014). Contaminant load variations and high regeneration costs reduce the effectiveness of the adsorption process (Jo & Yang, 2009). Thus, overall, the use of conventional gaseous contaminants abatement techniques is limited by the features of secondary waste generation and high operation costs (Krishnamurthy et al., 2019; Luengas et al., 2015). The merits and demerits of some of the aforementioned conventional processes for gaseous pollutant removal are given in Table S1.

3. General overview of the removal of gaseous pollutants via photocatalytic oxidation

3.1. General mechanism of photocatalysis

People spend almost 80% of their life in indoor places such as residential units, offices, workshops, etc. Therefore, indoor air quality (IAQ) is vital for human health. In addition, outdoor air quality (OAQ), with pollutants produced mostly from industrial pollution/human activities, can cause major environmental, medium-term, and long-term health problems such as respiratory diseases (e.g., emphysema), heart damage, lung cancer, sudden death and cognitive alterations (Olmo et al., 2011). As already reported in section 2, we see that all the current, conventional gaseous contaminants abatement techniques have significant limitations.

The photocatalytic oxidation of gaseous pollutants, including volatile organic compounds (VOCs) (Ardizzone et al., 2008; Ganesh et al., 2011; Lopes et al., 2012; Monteiro et al., 2015) or inorganic gaseous (e.g., NO_x (Ballari et al., 2010; Zouzalka & Rathousky, 2017), SO_x (Li et al., 2016) and H₂S (Navakoteswara Rao et al., 2019) is a promising technology not least because in many cases it produces less-toxic and odorless compounds and can utilise solar radiation. The photocatalytic oxidation reaction is focused on the production of reactive oxygen species (ROs) having high oxidizing potentials such as HO•, O₂•⁻, HO₂•⁻, and H₂O₂⁻, which can oxidize water- or air-borne pollutants adsorbed on the surface of photocatalyst. In SPC it is also possible to oxidize adsorbed pollutants directly, via their reaction with photogenerated valence band holes (h⁺) on the surface of the photo-excited photocatalyst can take place as well (Djellabi et al., 2020). As showed in Figure 2A, unlike the extensive use of photocatalysis for water treatment, less attention has been given to the application for heterogeneous photocatalysis for air purification over the last two decades. Figure 2B shows the mechanistic pathways of organic pollutant removal via their photocatalytic oxidation over photocatalyst surface sites.

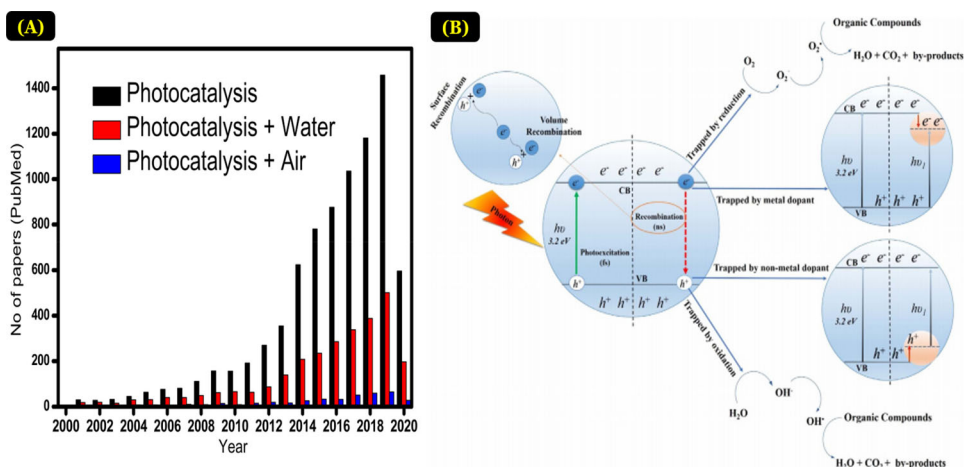


Figure 2. (A) Publications trends in photocatalysis, photocatalysis for water and air treatment over the last two decades, obtained from PubMed (up to Apr. 2020) (B). Photocatalytic oxidation of organic pollutants, including gas substances, by heterogenous photocatalysis process (Adapted with permission from ref (Shayegan et al., 2018), copyright 2017 Elsevier).

3.2. Parameters affected the photocatalytic efficiency

The efficiency of the photocatalytic degradation of gas pollutants depends upon many factors. Since the production of $HO\bullet$ is carried out via the reaction of adsorbed water or HO^- with positive holes, in air medium, relative humidity (RH) is a key reaction parameter (Amaterz, Tara, Bouddouch, Taoufyq, Bakiz, Benlhachemi, et al., 2020; Amaterz, Tara, Bouddouch, Taoufyq, Bakiz, Lazar, et al., 2020; Guo et al., 2008; Mamaghani et al., 2017) which can affect the overall rate of photocatalysis greatly (Aghighi & Haghghat, 2015). For example, a high relative humidity can prevent/inhibit the adsorption of gas compounds, reducing their chance of being oxidized photocatalytically and yet at more modest levels it is essential for effective SPC. For example, Korologos et al. (2011) has reported that the presence of water enhances the oxidation of benzene and toluene effectively but without water vapour present no pollutant removal was possible.

Airflow is another important factor that shows a dual antagonistic effect on SPC efficiency (Shayegan et al., 2018). Thus, for low airflow rates, the residence time of pollutants on the surface of the photocatalyst and in the reactor is high and so provides the pollutant species in the gas phase and increased opportunity to be adsorbed on the photocatalyst's surface and undergo reaction by the photo produced ROSs and/or h^+ 's. However, at higher airflow rates, the shorter residence time will decrease the likelihood of reaction, resulting in a lower oxidation/mineralization efficiency. Therefore, in the photocatalytic reactor, the airflow should be optimized to obtain an optimum photocatalytic efficiency depending on the reactor and

the operating conditions employed, such as the gas contaminant concentration. In addition, the airflow rate may also affect the formation of the by-product during photo-oxidation of contaminants and the total oxidative mineralization to CO_2 (Farhanian et al., 2013; Sleiman et al., 2009; Yang et al., 2015).

The type of photocatalyst employed is also key in deciding the efficacy of the photocatalytic oxidation process in water or air phases. Thus, for more than three decades, most scientific research has been carried out to develop photoactive materials and nanomaterials for environmental remediation and energy production, especially to enhance the adsorption capacity, improve the visible light response, and reduce the recombination of photo-generated electron/hole pairs. Several strategies have been employed, such as the modification of photocatalysts (e.g., TiO_2) by metal (Karafas et al., 2019; Nie et al., 2019) and nonmetal doping (Jo & Kim, 2009; Patil et al., 2019), the combination of semiconductors with high adsorbing materials (Shayegan et al., 2020), photosensitizing (Park et al., 2013; Xiao et al., 2008) and coupling of semiconductors (Djellabi, Yang, Xiao, et al., 2019; Djellabi, Yang, Adeel Sharif, et al., 2019). So far, a wide variety of titania and non-titania-based photocatalysts have been employed for air purification (Boyjoo et al., 2017). Many physicochemical factors must be taken into consideration for developing a photocatalyst for air treatment, such as increasing the visible light activity, enhancing the selectivity toward some pollutants (e.g., NO_x), and improving gaseous phase pollutants mineralization into preferred products (CO_2 , H_2O , and inorganic species) and avoiding the formation of unwanted coke on the surface of the photocatalyst, resulting in its deactivation.

The type and the concentration of the gas pollutant significantly affect the photocatalytic oxidation efficiency. Indeed, the photooxidation efficiency depends on the photocatalyst's affinity toward the type of pollutant, wherein species showing good adsorption on the photocatalyst have more possibility to be oxidized (Jafarikojour et al., 2015; Mamaghani et al., 2017; Zhong et al., 2013). More by-products are likely to be produced at higher pollutant concentrations, and in some cases this will impede the overall mineralization process. Therefore, photocatalysis for air purification is usually more effective when carried out using low concentrations of contaminants although this will also depend upon the photocatalyst's surface chemistry and porosity.

One of the successful applications of photocatalysis for air treatment has been the development of self-cleaning photo-materials. These smart materials have been applied for different purposes, such as house furniture and glasses, roofs, solar panel cleaning, cement, and self-cleaning building (Banerjee et al., 2015; Ganesh et al., 2011). Under solar light, self-cleaning

materials can remove adsorbed gas contaminants/or bacteria via the process of SPC, coupled with the action of rain, and then by the action of rain, clean themselves. A number of different self-cleaning materials have been developed to remove various gas phase contaminants (Ardizzone et al., 2008, 2007; Bianchi et al., 2020, 2016, 2014; Cappelletti et al., 2008).

Many semiconductor composite photocatalysts with different geometrical configurations and compositions have been extensively synthesized and applied to the oxidation of various gaseous phase pollutants. Table S2 (see [Supplementary material](#)) summarizes the recent studies of representative composite semiconductor photocatalysts for removing many types of pollutants in the gas phase.

3.3. Photocatalytic reactors for air treatment

The photocatalytic reactor type and its geometry are also significant factors for air purification since they can influence directly the contact of contaminants with the immobilized photocatalyst (Boyjoo et al., 2017). For this purpose, many photo-reactor configurations have been designed for contaminants oxidation in the gas phase, such as packed bed (Lopes et al., 2012), annular reactor (Monteiro et al., 2015), flat plate reactor (Passalía et al., 2017), honeycomb monolith (Taranto et al., 2009), and multiplate/annular (Zazueta et al., 2013). In order to improve the value of the surface of coated photocatalyst per volume of the reactor ratio, which in turn enhances the uniform irradiated photocatalyst surface and the mass transfer, researchers have developed a new microreactor based on NET mix technology for the oxidation of VOCs in the gas phase (da Costa Filho, Araujo, et al., 2019; da Costa Filho, Silva, et al., 2019; da Costa Filho et al., 2017) (see [Supplementary Figure S1](#)).

4. General overview of Ag_3PO_4 photocatalyst

4.1. Crystal structure of Ag_3PO_4 photocatalyst

Ag_3PO_4 is a cubic crystal structure with a space group (P4-3n) and parameter lattice $\approx 6.004 \text{ \AA}$. Isolated, regular PO_4 tetrahedrals create a body-centered cubic lattice, with a P-O distance is $\approx 1.539 \text{ \AA}$. The Ag^+ ions are dispersed between twelve sites with double symmetry (Ng et al., 1978). Every Ag atom on the 2-fold axis mainly uses one of the two sites at (x,0, 0.50) and (0.5-x, 0, 0.50). The Ag atom has 4-fold coordination by four O atoms (Ma et al., 2011). The P atoms experience 4-fold coordination encircled by four atoms of O, while O atoms experience 4-fold coordination encircled by three atoms of Ag and one atom of P (Kahk et al., 2014) (see [Supplementary Figure S2](#)).

Kahk et al. (Kahk et al., 2014) reported that the lattice parameter of Ag_3PO_4 acquired theoretically from DFT calculations is 6.072 Å. In addition, Ma et al. (Ma et al., 2011) concluded that Ag_3PO_4 with polyhedron configuration mainly contains tetrahedral AgO_4 and PO_4 . They stated that three AgO_4 and one PO_4 are joint over the corner oxygen. They explained that Ag_3PO_4 photocatalytic activity is due to PO_4^{3-} ions owing to its higher negative charge, thus maintaining a large dipole in the Ag_3PO_4 , resulting in the distortion of AgO_4 (Ma et al., 2011).

4.2. Electronic structure of Ag_3PO_4 photocatalyst

In order to have a better understanding of the source of the photocatalytic activity of Ag_3PO_4 , a thorough electronic study is essential. An analysis of the ultraviolet-visible diffuse reflectance spectrum indicates the indirect and direct transition bandgap energies of Ag_3PO_4 are 2.36 eV and 2.43 eV, respectively (Yi et al., 2010). Therefore, Ag_3PO_4 can adsorb illumination under visible light with an average wavelength (< 530 nm).

Using density functional theory (DFT), several studies have been carried out in order to better understand Ag_3PO_4 's high photocatalytic activity (see [Supplementary Figure S3.A](#)). For example, Ma et al. (2011) reported that Ag_3PO_4 has a conduction band with large dispersion that enables the separation of charge carriers. Furthermore, the vacancies present in Ag_3PO_4 could play a significant role in the separation of the electron-hole pairs.

Liu et al. (2011) also reported that Ag_3PO_4 has a bandgap energy of 2.43 eV (see [Supplementary Figure S3.B](#)). The conduction and valence bands mainly consisting of (Ag 5s, 5p) and (O2p, Ag 4d) states, respectively. A VBM potential of 2.67 eV implies a sufficient driving force for the oxidation of water and the direct oxidation of most pollutants.

Xu et al. (2014) studied Ag_3PO_4 and graphene (GR) surface interaction and established good stability and electron transfer mechanism along with the photocatalytic activity. The strength of interfacial interaction is attributed to the geometry and separation of $\text{Ag}_3\text{PO}_4/\text{GR}$.

Kahk et al. (2014) demonstrated that the prediction of the electronic, structural, and optical characteristics of Ag_3PO_4 using DFT calculations was consistent with experiment. Molecular orbital (MO) theory was used to propose an interpretation of the electronic structure of Ag_3PO_4 (see [Supplementary Figure S3.C](#)) and the results suggests that the covalent interactions between silver and oxygen are weaker than those between phosphorus and oxygen, commencing from an isolated $(\text{PO}_4)^{3-}$ unit, a molecular orbital diagram for Ag_3PO_4 was created. In this work, only sigma interactions between orbitals over O and P were considered for $(\text{PO}_4)_3^-$,

two orbitals of sigma symmetry were provided by four oxygen atoms: 2 s and one of the three 2p. The two triply degenerate ligand group orbital (LGO) is t₂ symmetry, and two LGO of a₁ symmetry in a tetrahedral environment. These overlap with the P 3s (a₁) and P 3p (t₂) orbitals and form twelve molecular orbitals, as demonstrated in (see [Supplementary Figure S3.C](#)).

4.3. Photocatalytic properties of Ag₃PO₄ photocatalyst

Key factors responsible for a high photocatalytic activity for air purification include (i) the successful photo-excitation and the formation of separated electron/hole pairs during visible or UV irradiation, especially promising if this can be effected using visible light; (ii) the ability of the photocatalyst photogenerated conduction band electrons to reduce dissolved O₂ to superoxide (Wood, 1988); (iii) the ability of the photogenerated valance band holes to oxidize H₂O or adsorbed ⁻OH into [•]OH radicals ($E_0(\text{H}_2\text{O}/\text{HO}^\bullet) = 2.73 \text{ V}$ vs the NHE; $E_0(\text{HO}^-/\text{HO}^\bullet) = 1.9 \text{ V}$ vs the NHE) (Schneider et al., 2014); (iv) the interaction of the surface area with the pollutant under test, since the photocatalytic mineralization process takes place at photocatalyst surface sites, (thus, adsorbed pollutants have more chance of being oxidized via ROSs (Djellabi et al., 2020); (v) the stability of the photocatalyst is also considered as a critical key for practical application.

Since 2010, Ag₃PO₄ has been identified as a photocatalyst for organic pollutant oxidation and water splitting (Yi et al., 2010). Ge et al. (2012) reported that the scavenging of HO[•] and [•]O₂⁻ species by isopropyl alcohol and benzoquinone, respectively, does not affect visible-light-driven RhB photocatalytic degradation using Ag₃PO₄, thereby prompting these workers to suggest that the latter ROSs do not contribute much to the oxidation of RhB. In other words, the photo-production of HO[•] and [•]O₂⁻ via the Ag₃PO₄/visible light system is not very efficient. They reported that the CB and VB are not thermodynamically able to convert O₂ into O₂^{•-} and H₂O into HO[•] and HO[•]. However, the photocatalytic degradation of RhB was utterly inhibited when EDTA was added to the reaction, which confirms that direct oxidation of RhB by photoinduced h⁺ on Ag₃PO₄ is the primary oxidation mechanism. Dong et al. (2016) also showed that the direct hole oxidation of MB by Ag₃PO₄ (oxidized at 200 °C) is the most crucial pathway, while there is also the participation of HO[•] species. As shown in [Figure 3A](#), Ag₃PO₄ is very effective for oxygen evolution via the oxidation of H₂O by the photogenerated holes and concomitant reduction of the sacrificial electron acceptor, Ag⁺, to Ag (Bierman et al., 2008).

As noted earlier, one of the main problems associated with using of Ag₃PO₄ as a photocatalyst for environmental remediation is the photo-

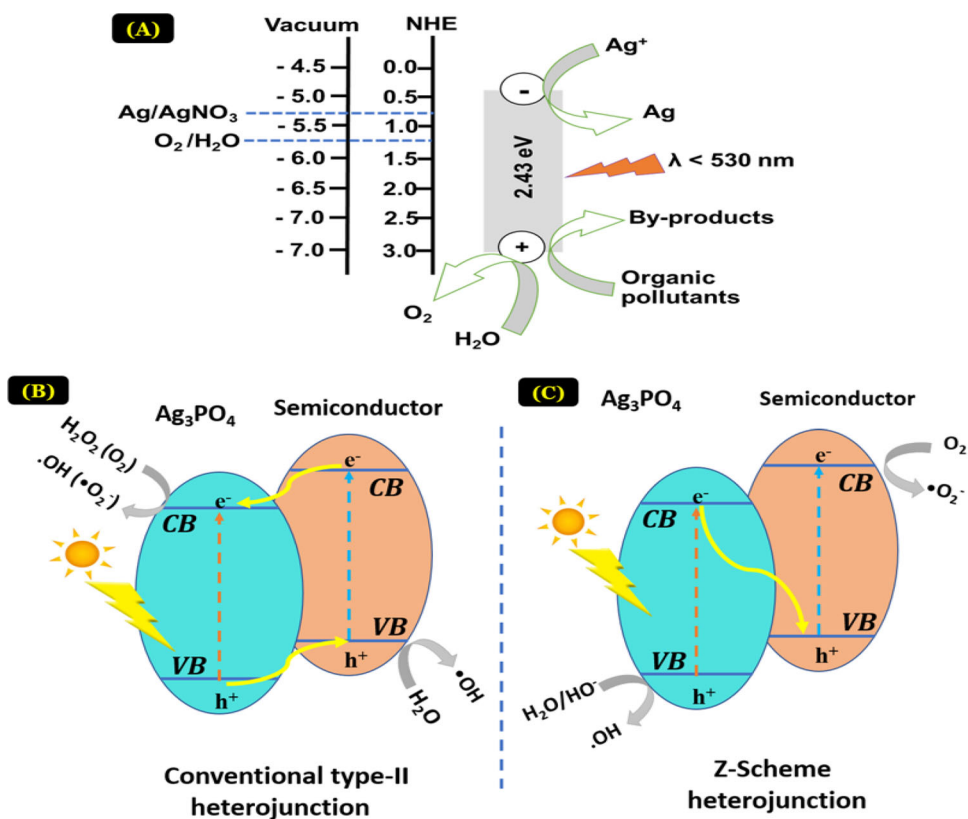


Figure 3. (A). Mechanistic pathway of photocatalytic oxidation of organic pollutants in Ag₃PO₄/visible light; (B) Schematic of the conventional type-II heterojunction; (C) Schematic of the Ag₃PO₄-Based Z-scheme heterojunction photocatalyst (inspired from (Xue et al., 2020; Yi et al., 2010)).

corrosion issue due to Ag⁺ reduction into metallic Ag (Martin et al., 2015), since this process leads to the deactivation of the photocatalyst. In addition, due to the position of its CB and VB potential edges, the efficiency of Ag₃PO₄ photocatalyst for photo-producing ROSs is very low. Thus only pollutants that are adsorbed on the Ag₃PO₄ surface have some possibility of being oxidized and ultimately oxidatively mineralized, and then by direct reaction with the photogenerated valence band. It is essential to point out that the specific surface area of Ag₃PO₄ is very small as reported by some studies, e.g., 0.98 m²/g (Yi et al., 2010); 0.16–1.02 m²/g (Dong et al., 2016); 2 m²/g (Ge et al., 2012).

5. Improving photocatalytic activities of Ag₃PO₄ photocatalyst toward the degradation of pollutants in gas-phase

The generation of by-products during the photocatalytic treatment process in both the purification of water and air is a major issue that represents a

barrier to the widespread application of photocatalysis systems for pollution control in the real-world (Pichat, 2019). This problem is somewhat reduced in that the photocatalytic system can continuously produce ROSs, so as to eventually mineralize such by-products. But, in general, photocatalysis cannot be used as a single treatment process when it comes to the real application due to its shortcoming in terms of the formation of by-products. Therefore, the combination of photocatalysis with other pollutant removal systems is crucial in order to create a highly effective air purification system.

The formation of heterojunctions between Ag_3PO_4 and other semiconductors is an attractive option help reduce its tendency to undergo photo-induced corrosion and create a photocatalytic system with characteristics which are different to the that of a single photocatalyst (Cai et al., 2020; Tang et al., 2020). A prolonged carrier lifetime and an enhanced interfacial charge transfer rate can be obtained from such heterostructures. However, it is also well understood that it is not easy to get the desired properties for the heterojunctions and will depend strongly on the degree of matching of the valence and conduction bands of the component semiconductors (Lu et al., 2015; Wang et al., 2015).

Ag_3PO_4 -Based Z-scheme and conventional heterojunctions have already been extensively investigated to the enhance photo-generation of the charges responsible for the desired photocatalytic reactions and inhibit any photo-corrosion (Chen et al., 2014; Lu et al., 2015; Rao et al., 2020; Tang et al., 2020). The type II junction is the most common in conventional heterojunctions (Figure 3B). In contrast, the newly emerged direct Z-scheme heterojunction (Figure 3C) is regarded as the most efficient in Z-scheme systems to explore photo-generated carriers (He et al., 2018). Both heterojunctions have different charge carrier transport mechanisms, but the structure of both direct Z-scheme and type-II heterojunctions is the same.

The formation of conventional type-II heterojunction is mainly dependent on combining the two different semiconductors (SC-I) and (SC-II) which have an appropriate CB and VB band structure for the transfer of photogenerated electrons and holes Figure 3B. Upon ultra bandgap irradiation, due to the electron fields within the heterojunction, the photogenerated electron and holes from SC-I and SC-II can move toward SC-II (CB) and SC-I (VB), respectively. As a consequence, electron-hole pair recombination associated with the individual semiconductors is reduced, and surface oxidation and reduction reactions promoted over the two semiconductors. (Huang et al., 2019; Lam et al., 2012; Pirhashemi et al., 2018). In contrast, a completely different mechanism of charge carrier migration can also occur in the case of direct Z-scheme heterojunctions. In this case, upon irradiation, the electron produced on semiconductor II (SC-

II) transfers toward the higher reduction potential of semiconductor I (SC-I) (Figure 3C), while the photogenerated holes remain on semiconductor II (SC-II), resulting in the spatial separation of charge carriers, thereby producing an overall very effective separation of a photogenerated electron and hole. As a result, a direct Z-scheme heterojunction photocatalyst has the potential to create a system with an enhanced the photocatalytic activity (He et al., 2018; Huang et al., 2019). The direct Z-scheme heterojunction photocatalyst offers two obvious merits, a highly efficient photogenerated electron hole pair separation and so high photocatalytic activity and a low-cost fabrication (Huang et al., 2019; Low et al., 2017; Zhou et al., 2014).

The bottom of the Ag_3PO_4 conduction band (CB) energy level is more positive than the reduction potential of O_2 ($\text{O}_2 + e^- \rightarrow \bullet\text{O}_2^-$, -0.33 V vs. NHE) (Wood, 1988). Therefore, introducing another semiconductor to produce the Z-scheme system is beneficial for the degradation of gaseous pollutants and the extension of Ag_3PO_4 lifetime if the photo-excited electrons in the CB of Ag_3PO_4 can be transferred efficiently to the second introduced semiconductor photocatalyst.

A wide range of Ag_3PO_4 -based heterojunctions photocatalysts have been generated through various well-established synthesis protocols and then used for the photocatalytic oxidation of gas-phase pollutants and many of the systems are described below.

5.1. Coupling Ag_3PO_4 with graphitic carbon nitride ($g\text{-C}_3\text{N}_4$)

Graphitic carbon nitride ($g\text{-C}_3\text{N}_4$) has gained considerable interest as a metal-free polymer n-type semiconductor due to favorable characteristics such as its 2D structure, tunable electric structure, and good chemical stability. It is a visible-light-driven semiconductor (2.7 eV bandgap), with CB and VB energy position at -1.1 and 1.6 eV vs. standard hydrogen electrode (NHE), respectively (Che et al., 2020; Dong et al., 2014; He et al., 2020; Masih et al., 2017; Tian et al., 2017). These characteristics make $g\text{-C}_3\text{N}_4$ the most attractive candidate for use in a Z-scheme system for the highly efficient photocatalysis of gas-phase volatile pollutant degradation.

There are several reports of such Z-scheme systems regarding the degradation of gaseous pollutants. They include the photocatalyzed destruction of volatile organic pollutants (toluene, Ethylene, isopropanol, formaldehyde) and nitrogen oxide (NO_x) by an $\text{Ag}_3\text{PO}_4/g\text{-C}_3\text{N}_4$ composite photocatalyst (Chen et al., 2014; Rao et al., 2020; Shen et al., 2018; Zhao et al., 2017). Thus, Chen and his coworkers (Chen et al., 2014) recently prepared a direct Z-scheme configuration-based novel $g\text{-C}_3\text{N}_4/\text{Ag}_3\text{PO}_4$ composite for visible-light-driven (300 W Xe lamp) photocatalytic oxidation of ethylene (C_2H_4). The results indicate that the coupling of $g\text{-C}_3\text{N}_4$ with Ag_3PO_4

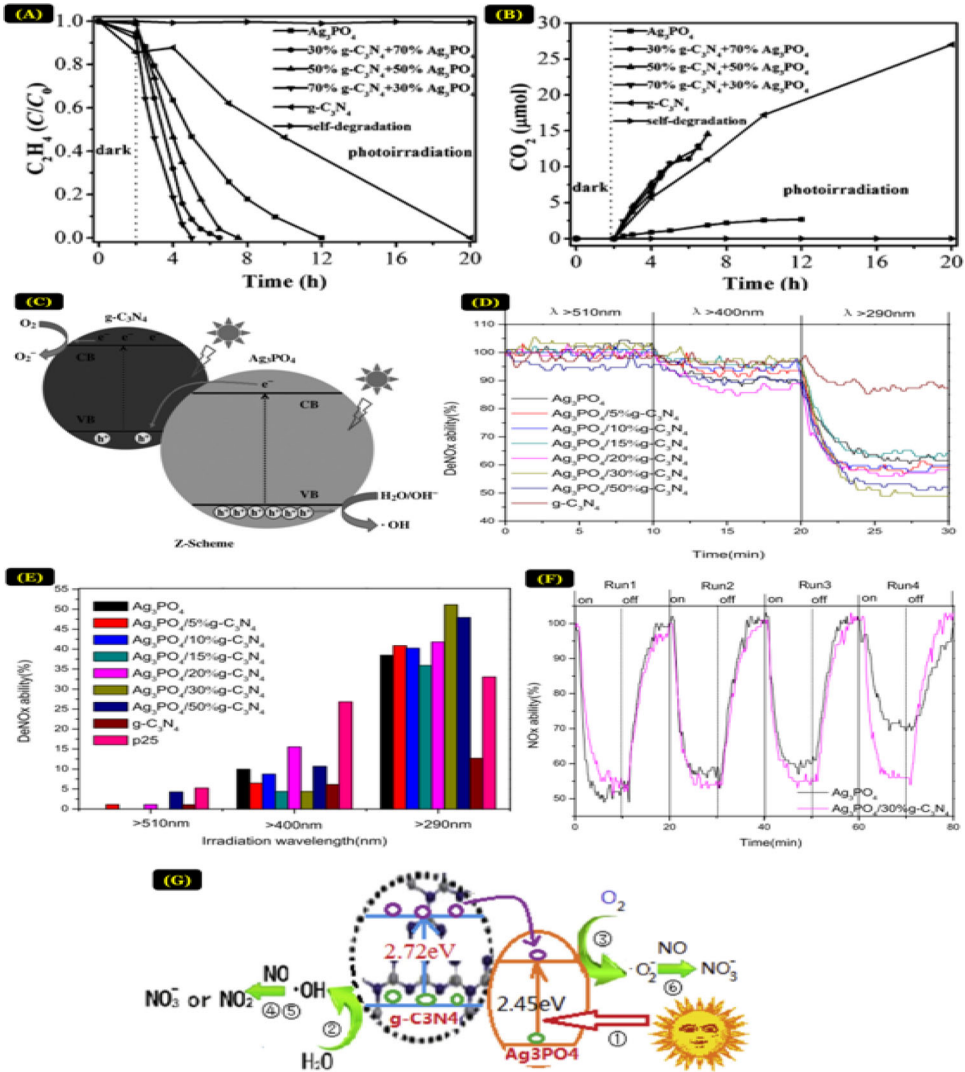


Figure 4. Time courses of (A) C_2H_4 degradation and (B) CO_2 evolution on $g-C_3N_4$ - Ag_3PO_4 composites, (C) Charge transfer in the $g-C_3N_4$ - Ag_3PO_4 Z-Scheme mode under sunlight illumination (Figures 4A,4B and 4C are adapted with permission from ref. (Chen et al., 2014), copyright 2014 Wiley Online Library). (D) and (E) NOx destruction activities of $Ag_3PO_4/g-C_3N_4$ composites under the irradiation of different wavelengths of light, (F) Cycling photocatalytic degradation of NOx under 290 nm irradiation, (G) the possible mechanism of visible-light-induced photocatalysis of $Ag_3PO_4/g-C_3N_4$ composite (Figures 4D,4F,4E and 4G are adapted with permission from ref. (Zhao et al., 2017), copyright 2016 Elsevier).

resulted in enhanced gas adsorption. Notably, by using (30:70%) ratio of Ag_3PO_4 and $g-C_3N_4$ composite, the complete decomposition of C_2H_4 (90 μL) was achieved after 3 h under visible light, whereas bare Ag_3PO_4 needs 20 h for complete decomposition of C_2H_4 under visible light irradiation (Figure 4A). Moreover, it was noted that $g-C_3N_4$ - Ag_3PO_4 composites exhibited higher rate constants ($1.0464 h^{-1}$) than that exhibited by pristine

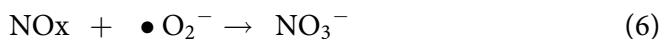
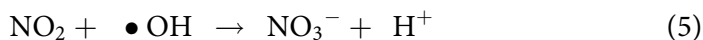
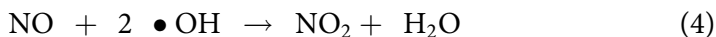
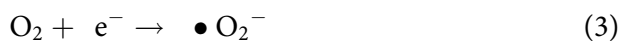
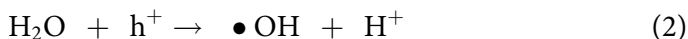
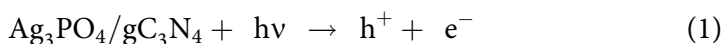
g-C₃N₄ (12.38 times lower) and Ag₃PO₄ (3.7 times lower). Hence, it is confirmed that the synergetic combination of Ag₃PO₄ and g-C₃N₄ improves photogenerated charge carrier separation and in so doing produces a superior photocatalytic performance. Furthermore, It was observed that during the photo-oxidation of C₂H₄, no other products except CO₂ were detected (Figure 4B). The fact that the CO₂ yields for all g-C₃N₄-containing samples were greater than that which can be generated from C₂H₄ reveals an obvious adsorption effect of g-C₃N₄. Moreover, this composite was stable for the photocatalytic oxidation of C₂H₄ and could be recycled upto 5 times without exhibiting a significant decrease in its activity.

According to their investigation, the reaction mechanism under sunlight illumination during ethylene photocatalytic oxidation using 70% g-C₃N₄-30% Ag₃PO₄ catalysts may be summarized by the schematic presented in Figure 4C. Thus, upon sunlight irradiation, a photogenerated conductance band electron on Ag₃PO₄ (CB) transfers to the photoexcited g-C₃N₄ (VB) and there reacts with one of its photogenerated holes, thus resulting in efficient removal of the photo-generated electron from the Ag₃PO₄, thereby preventing its reaction with the Ag⁺ ions. Meanwhile, the highly reducing, photogenerated conductance band electrons on g-C₃N₄ react readily with surface adsorbed O₂ to produce superoxide. In order to stay electrically neutral the remaining photogenerated holes on the Ag₃PO₄ react either with surface water to produce OH radiacals or directly with any surface adsorbed organic pollutant, C₂H₄, thereby oxidizing it. The overall process is a 2 photon photocatalyzed oxidative mineralization of the C₂H₄ by O₂; by coupling the Ag₃PO₄ with g-C₃N₄ the Ag₃PO₄ is rendered much more stable (Chen et al., 2014).

A number of different Ag₃PO₄/g-C₃N₄ composites have also been made by a simple in-situ solvothermal process with different mass ratios (1:0, 19:1, 9:1, 17:3, 4:1, 7:3, and 1:1) of C₃N₄ and the composites used, under different irradiation conditions, for the photocatalyzed decomposition of NO_x (Zhao et al., 2017). The results reveal no apparent NO_x destruction at 510 nm wavelength using both Ag₃PO₄ or g-C₃N₄ (Figure 4D), however, NO_x decomposition under irradiation of >400 nm was observed using Ag₃PO₄/20%gC₃N₄, Ag₃PO₄/30%g-C₃N₄, and Ag₃PO₄/50%g-C₃N₄ composites photocatalysts with average performance rate of 15.52%, 4.35%, 10.64%, respectively (Figure 4D). In addition, by fixing the irradiation wavelength at 290 nm, an incremental increase in activity was observed of all the composites for the photocatalytic decomposition of NO_x, with average decomposition rates of 41.76%, 51.09% and 47.87%, respectively, see (Figure 4D). These decomposition rates were comparatively higher than those observed for pristine g-C₃N₄, Ag₃PO₄, and P25, thus demonstrating the promising efficiency of the Ag₃PO₄/g-C₃N₄ composite under both

ultraviolet and visible irradiation due to enhanced light absorption after Ag_3PO_4 and $\text{g-C}_3\text{N}_4$ composite formation (Figure 4E). It was also noted that under irradiation $>290\text{ nm}$, the system exhibited excellent stability, and that the remarkable efficiency of the $\text{Ag}_3\text{PO}_4/30\%\text{g-C}_3\text{N}_4$ photocatalyst continued even after four cycles. In contrast, the NO_x decomposition rate of Ag_3PO_4 alone decreased with repeated use (Fig. 4F). The results of this work suggest that the $\text{g-C}_3\text{N}_4$ addition automatically improves Ag_3PO_4 stability and inhibits its photo-corrosion.

The photocatalytic mechanistic pathways on $\text{Ag}_3\text{PO}_4/\text{g-C}_3\text{N}_4$ photocatalysts under visible light is illustrated in Figure 4G. When $\text{Ag}_3\text{PO}_4/\text{g-C}_3\text{N}_4$ photocatalysts composite is irradiated by visible light (Eq. (1)), the transfer of photoexcited electron occurs from $\text{g-C}_3\text{N}_4$ CB to Ag_3PO_4 , inhibiting electron and holes recombination behavior. Thus, the hole present over the $\text{g-C}_3\text{N}_4$ valence band (VB) is scavenged by water molecules to generate more free hydroxyl radical ($\text{OH}\bullet$) (Eq. (2)). Conversely, the photogenerated and transfer electrons over the Ag_3PO_4 CB site automatically react with oxygen, thereby generating oxygen radicals (Eq.(3)) and resulting in the oxidation of nitrogen monoxide via oxygen, hydroxyl radical, and water producing NO_2^- or NO_3^- . Moreover, it was noted that during light irradiation, only 20% of NO was converted into O_2 and N_2 , while the rest 80% was oxidized to NO_3^- . The overall mechanism of photocatalytic NO_x decomposition via $\text{Ag}_3\text{PO}_4/\text{g-C}_3\text{N}_4$ composite under visible light is presented below (Zhao et al., 2017):



Similarly, Rao et al. (2020) proposed a different mass ratio (0.5, 1.0, 1.5, to 2.0 wt%) to prepare $\text{Ag}_3\text{PO}_4/\text{g-C}_3\text{N}_4$ nanocomposites. In a continuous flow system, irradiated with a 420 nm LED, the photocatalyzed oxidative mineralization of formaldehyde (HCHO) (0.5 mg/m^3) was studied using a $\text{Ag}_3\text{PO}_4/\text{g-C}_3\text{N}_4$ photocatalyst (Rao et al., 2020). The results of this work showed maximum formaldehyde degradation rates (8.51%, 10.60%, 22.4%, 10.60%, and 6.38%), in the order of $\text{g-C}_3\text{N}_4$, 0.5AP-CN, 1AP-CN, 1.5AP-CN, and 2AP-CN, respectively Figure 5A. The optimum photoactivity of the 1AP-CN heterojunction for HCHO degradation was about (2.63) times faster than $\text{g-C}_3\text{N}_4$. From the results of this work these researchers suggest that when Ag_3PO_4 as an impurity semiconductor is inserted into the g-

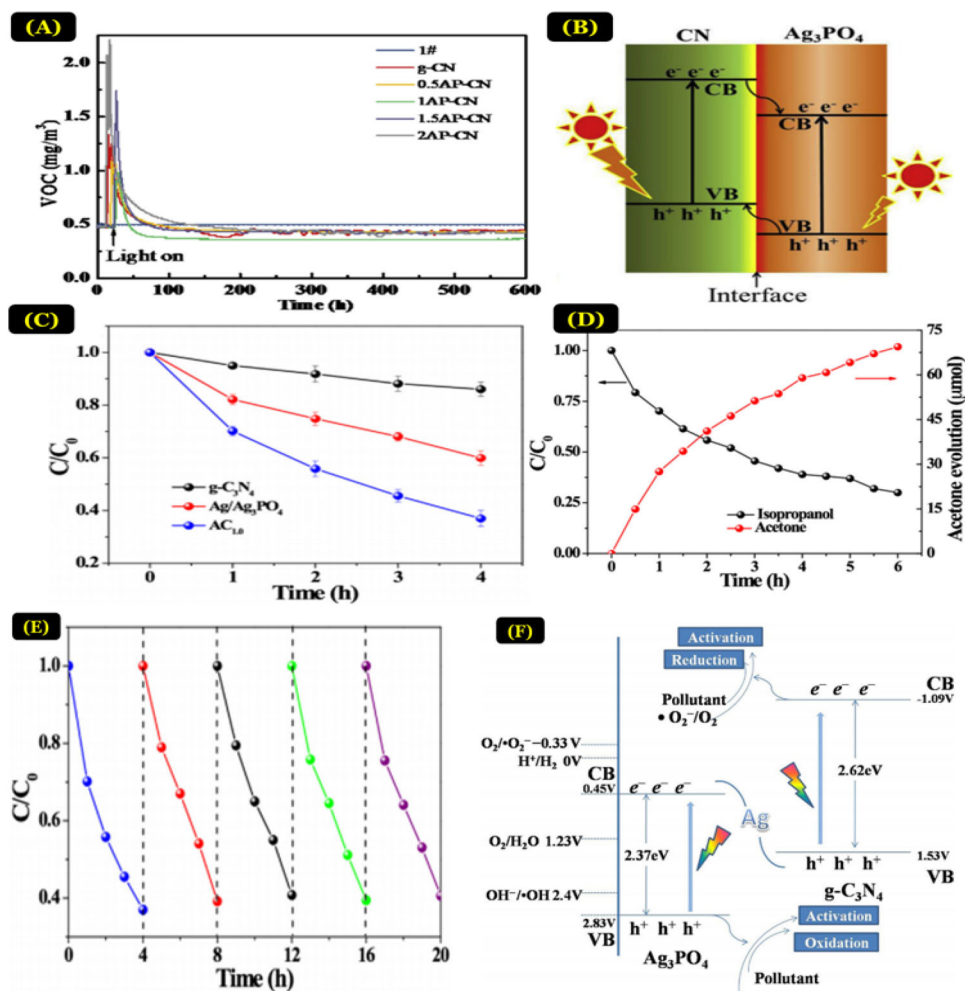


Figure 5. (A) Degradation measurement of flowing gas-phase formaldehyde (B) Energy band schematic of $\text{Ag}_3\text{PO}_4/\text{g-C}_3\text{N}_4$ composites (Figures 5A and 5B are adapted with permission from ref. (Rao et al., 2020), copyright 2019 Elsevier). (C) Photocatalytic degradation of gaseous isopropanol over $\text{AC}_{1.0}$, $\text{Ag}/\text{Ag}_3\text{PO}_4$ and $\text{g-C}_3\text{N}_4$ samples, (D) Photocatalytic degradation of gaseous isopropanol and amounts of acetone evolution yield over $\text{AC}_{1.0}$, (E) the cyclic stability tests of $\text{AC}_{1.0}$, (F) Schematic illustration for the charge transfer and separation in Z-scheme $\text{g-C}_3\text{N}_4/\text{Ag}/\text{Ag}_3\text{PO}_4$ photocatalytic composite under visible-light irradiation (Figures 5C,5D,5E, and 5F are adapted with permission from ref. (Shen et al., 2018), copyright 2018 Elsevier).

C_3N_4 lattice, type II heterojunctions are created (Figure 5B), which can restrain photogenerated carriers recombination thereby enhancing the overall efficiency of the reaction. Moreover, their results reveal that under visible light irradiation, the photogenerated electrons trapped by O_2 over conduction band CB produce more $\bullet\text{O}_2^-$ radicals, and the presence of holes over the valence band (VB) directly participate in the oxidation of water/ OH^- and/or water by generating $\bullet\text{OH}$ radicals and thereby resulting in further oxidation of HCHO into H_2O and CO_2 .

In another study, Z-scheme g-C₃N₄/Ag/Ag₃PO₄ composites were used to promote the photocatalytic oxidation of gaseous isopropanol (Shen et al., 2018). The formation of g-C₃N₄/Ag/Ag₃PO₄ composites at room temperature was carried via a simple in situ deposition method by coating regular rhombic dodecahedrons Ag₃PO₄ particles over a g-C₃N₄ sheet. Later on different Ag₃PO₄ to g-C₃N₄ ratio were created, denoted by AC_x and x refer to various ratios (x = 0.3, 0.5, 0.7, 0.9, 1.0 and 1.2). The photocatalytic oxidation efficiency of AC1.0 (90 μL) was found to be the highest amongst the following photocatalysts Ag/Ag₃PO₄ and g-C₃N₄ (Figure 5C). In the case of AC1.0 samples, almost 63% IPA was removed within 4 h, higher than that by g-C₃N₄ (14%) and Ag/Ag₃PO₄ (40%). Their findings also showed that acetone was the main product during the photocatalytic oxidation of isopropanol. The incremental increase in acetone concentration was attributed to isopropanol's selective oxidation to acetone (Figure 5D). As depicted in Figure 5E, g-C₃N₄/Ag/Ag₃PO₄ as a photocatalyst for isopropanol oxidation exhibited significant efficiency over five consecutive cycles, thereby indicating a high stability of the studied photocatalyst. A schematic of the mechanism for the photocatalyzed oxidation of formaldehyde by g-C₃N₄/Ag/Ag₃PO₄ is shown in Figure 5F.

5.2. Coupling Ag₃PO₄ with TiO₂

TiO₂ continues to attract attention as an efficient UV light-driven photocatalyst, due to its nontoxic nature and low cost. Many attempts have been made by many researchers to construct a heterostructure of TiO₂ with Ag₃PO₄, not only to enhance the latter's stability but also to improve the overall photocatalytic activity exhibited by TiO₂ alone (Jia et al., 2019; Rawal et al., 2012; Xie et al., 2015; Zhao et al., 2014). For example, Rawal et al. (2012) created a novel Ag₃PO₄/TiO₂ heterojunction by coating Ag₃PO₄ surface sites with polycrystalline TiO₂ as illustrated in Figure 6A. The photocatalytic performance of the Ag₃PO₄/TiO₂ heterojunction under visible light irradiation ($\lambda \geq 420$ nm) was evaluated for the photocatalytic oxidation of gaseous 2-propanol (IP). The results showed that several compositions of Ag₃PO₄/TiO₂ composites exhibited photocatalytic activities greater than bare Ag₃PO₄ and TiO₂, (Figure 6B). The best of the composites, 3/97 Ag₃PO₄/TiO₂, was able to photocatalyse the oxidation of the 2-propanol within 120 min and the authors suggest that this enhanced activity was due to superior adsorption and higher photogenerated e⁻ transfer over interface between TiO₂ and Ag₃PO₄ (Figure 6B). In addition, photocatalytic activity was further evaluated in this system by monitoring the evolution of CO₂ as a function of irradiation time (Figure 6C) and revealed, once again, that the 3/97 Ag₃PO₄/TiO₂ photocatalyst was the

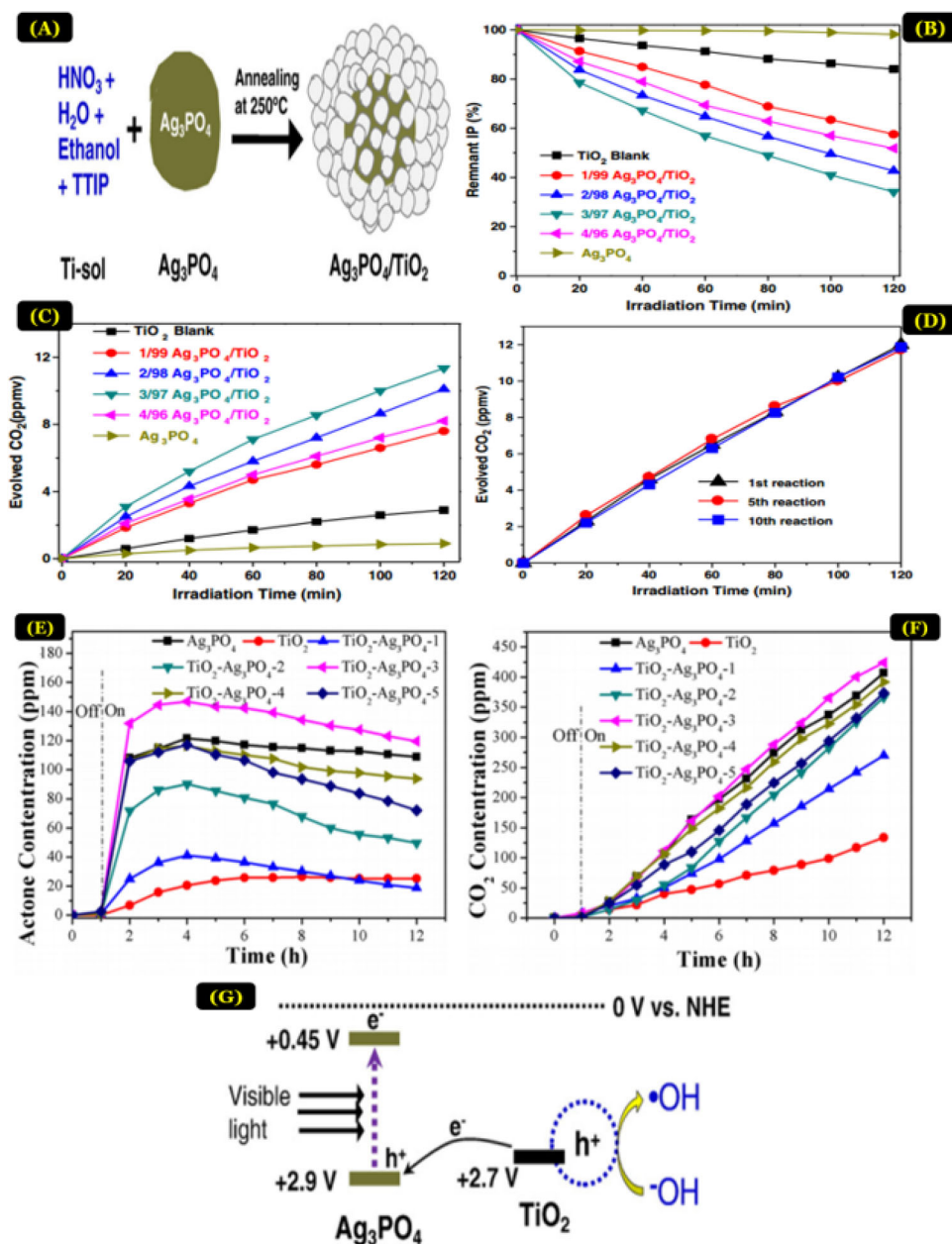
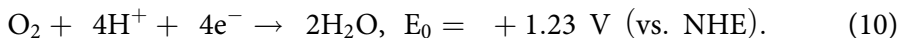
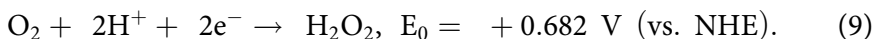
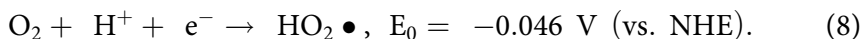
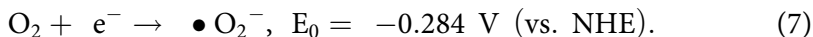
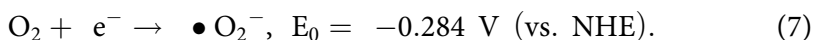


Figure 6. (A) Preparation strategy for $\text{Ag}_3\text{PO}_4/\text{TiO}_2$ composite; (B) Percentage of the remnant IP as a function of irradiation time in the presence of several $\text{Ag}_3\text{PO}_4/\text{TiO}_2$ composites under visible-light irradiation; (C) Amount of CO_2 evolved (ppmv) in the presence of several $\text{Ag}_3\text{PO}_4/\text{TiO}_2$ composites under visible-light irradiation, (D) Photocatalytic evolution of CO_2 by the repeated use of 3/97 $\text{Ag}_3\text{PO}_4/\text{TiO}_2$. (Figures 6A,6B,6C, and 6D are adapted with permission from ref. (Rawal et al., 2012), copyright 2011 Elsevier). Acetone (E) and (F) CO_2 evolution through degradation of 2-propanol by TiO_2 - Ag_3PO_4 photocatalysts (Figure 6E,6F are adapted with permission from ref. (Jia et al., 2019), copyright 2019 Elsevier). (G) Diagram for the charge carrier transfer and formation of $\bullet\text{OH}$ radical in the $\text{Ag}_3\text{PO}_4/\text{TiO}_2$ under visible light irradiation (Adapted with permission from ref. (Rawal et al., 2012). copyright 2011 Elsevier).

most active, generating 11.4 ppmv of CO₂ within 2 hour. In sharp contrast, the pristine Ag₃PO₄ and TiO₂ photocatalysts were only able to generate in the same irradiation time period 0.9 and 2.9 ppmv of CO₂, respectively. The stability of the 3/97 Ag₃PO₄/TiO₂ photocatalyst was evaluated for gaseous isopropanol decomposition and revealed change in the CO₂ vs irradiation time profile even after 10 cycles (Figure 6D), thus indicating a high photocatalytic stability.

Other workers also studied this system (Jia et al., 2019) i.e. the visible light driven photocatalytic decomposition of gaseous 2-propanol by Ag₃PO₄/TiO₂ nanocomposites. The observed high photocatalytic activities exhibited by the of Ag₃PO₄/TiO₂ composites obtained were attributed to their superior surface areas, which further enhances the visible light absorption capacity. Amongst the tested TiO₂-Ag₃PO₄ nanorods, TiO₂-Ag₃PO₄-3 (13% molar percentage of Ag₃PO₄) proved to be the best by producing ca. 147 ppm and 424 ppm of acetone and CO₂, within the first 3 h (Figure 6E) and 11 h (Figure 6F), respectively.

The proposed mechanism for the oxidation of 2-propanol by oxygen photocatalyzed by the Ag₃PO₄/TiO₂ nanocomposites is summarised in Figure 6G (Rawal et al., 2012). Thus, visible light irradiation produces an electron-hole pair on the Ag₃PO₄. The higher valence band position of Ag₃PO₄ (+2.9 eV vs. NHE) compared to TiO₂ enables the photogenerated valence band hole to transfer to the TiO₂, where it is able to oxidize the 2-propanol. Meanwhile, the photogenerated electrons on the Ag₃PO₄ is able to reduce O₂. However, when considering the latter redox reaction, it would appear that the direct reduction of O₂ to superoxide, reactions (7) or (8), is unlikely, on thermodynamic grounds (Krungchanuchat et al., 2017), and thus it is proposed that the reduction of O₂ by photogenerated conduction band electrons on Ag₃PO₄ involves multielectron transfer reactions (9) and (10).



5.3. Coupling Ag₃PO₄ with SrTiO₃

SrTiO₃ is one of the most commonly studied perovskite materials used in photocatalysis (Ji et al., 2019; Kong et al., 2016; Yue et al., 2018); it exhibits high corrosion resistance (Kong et al., 2016; Yue et al., 2018), high chemical stability (Kong et al., 2016), low cost (Kong et al., 2016), and is non-toxic (Kong et al., 2016; Zhang et al., 2010). It has also proved an efficient

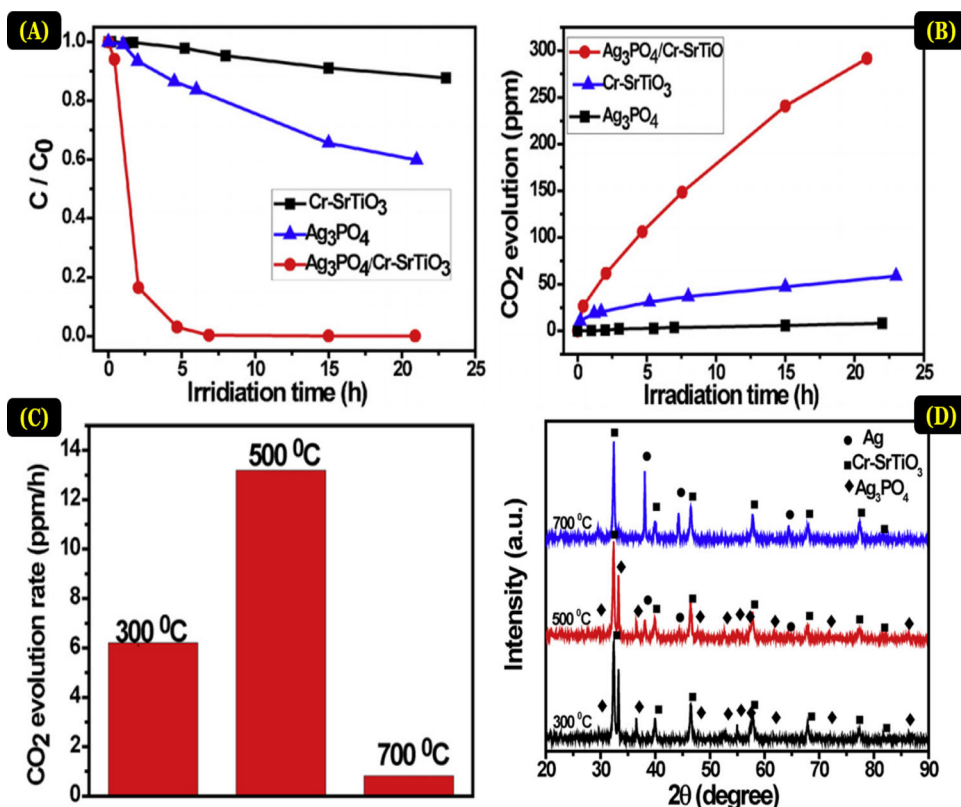


Figure 7. (A) The concentration change of IPA and (B) the evolution of CO_2 over $Cr-SrTiO_3$, Ag_3PO_4 and $Ag_3PO_4/Cr-SrTiO_3$ (1:4) composite powders under visible light irradiation; (C) the evolution rate of CO_2 under visible light irradiation of the $Ag_3PO_4/Cr-SrTiO_3$ (1:4) composite powders calcined at different temperature over ($420\text{ nm} < \lambda < 800\text{ nm}$); (D) The XRD patterns and Adapted with permission from ref. (Guo et al., 2013), copyright 2013 Elsevier.

photocatalyst for enhancing Ag_3PO_4 photocatalytic activity (Kong et al., 2016; Saadetnejad & Yildırım, 2018; Yue et al., 2018).

For example, in a study conducted by Guo et al. (2013), a novel $Ag_3PO_4/Cr-SrTiO_3$ heterojunction photocatalyst was used to promote the oxidation of isopropyl alcohol by O_2 using solar light ($420\text{ nm} < \lambda < 800\text{ nm}$). In this work $Ag_3PO_4/Cr-SrTiO_3$ samples with different ratios were used and their efficiencies as photocatalysts assessed by monitoring both the change in [IPA] and [CO_2] as a function of irradiation time. The best $Ag_3PO_4/Cr-SrTiO_3$ heterojunction composite was one with a (1:4) mass ratio which was able to photocatalyse the oxidation of 97% of the IPA within 3.8 h irradiation (Figure 7A). In contrast, pure Ag_3PO_4 and $Cr-SrTiO_3$ exhibited only 9% and 12% IPA decomposition within 8 h of irradiation, respectively (Figure 7A). In addition, and not surprisingly the highest rate of CO_2 evolution was found using this 1:4 $Ag_3PO_4/Cr-SrTiO_3$ heterojunction photocatalyst, which produced 291.2 ppm of CO_2 over 20 h of irradiation, which

was 35 and 5-fold higher than the bare Ag_3PO_4 and Cr-SrTiO_3 , respectively (Figure 7B). In this study, the effect of calcining the photocatalyst was also studied and revealed the highest photocatalytic activity was associated with 1:4 $\text{Ag}_3\text{PO}_4/\text{Cr-SrTiO}_3$ samples calcined over 500°C than the ones calcined over 300°C and 700°C (Figure 7C). XRD analysis of these calcined samples, see Figure 7D, suggest that the enhancement in activity may be due to the thermal production of metallic silver particles over the Ag_3PO_4 photocatalytic particles, which would act as efficient electron traps and catalysts for the reduction of O_2 via the multielectron processes described by Eqs. (9) and (10). In contrast, the decrease in photocatalytic performance with an increase in calcined temperature above 500°C , might be due to the decomposition of Ag_3PO_4 .

The group of Ji et al. (2019) investigated visible light induced Z-scheme photocatalysis exhibited by a $\text{Ag}_3\text{PO}_4/\text{Ag}/\text{SrTiO}_3$ composite, named $\text{AgPO}/\text{Ag}/\text{STO}$. In this work, using light with ($\lambda \geq 420\text{ nm}$, $150\text{ mW}/\text{cm}^2$), the photocatalysed destruction of different volatile organic compounds, ie. VOCs, which included xylene, toluene, and benzene, was studied mainly under above room temperature (RT) conditions, but not higher than 90°C . Their findings showed that the $\text{AgPO}/\text{Ag}/\text{STO}$ photocatalyst was able to destroy $> 90\%$ of the toluene vapor 800 ppm within 6 h of irradiation (Figure 8A), which was better than the AgPO/STO , Ag/AgPO , and Ag/STO photocatalysts. This work shows that the Ag NP bridge between the AgPO and STO photocatalysts enhances considerably photocatalytic performance. Other work showed that the rate of photocatalysis exhibited by the system increased with increasing temperature. Thus, the toluene conversion during the photo-thermo-catalytic oxidation (PTO) process significantly increased from (65%–94%) over $\text{AgPO}/\text{Ag}/\text{STO}$ as the temperature was increased from 45 to 90°C , see Figure 8B. In the absence of light, the (dark) thermal catalytic oxidation of toluene (TCO) was negligible and only the photocatalytic oxidation (PCO) was observed (Figure 8B). The photo-thermo-catalytic oxidation (PTO) activity exhibited by $\text{AgPO}/\text{Ag}/\text{STO}$ was also tested using xylene and benzene as the VOC. Their results showed that after 4 h photo-thermo-catalytic oxidation (PTO) process at 90°C , the conversion rates of xylene, toluene, and benzene were more than 85%, thereby suggesting its potential practical application.

A schematic of the proposed photocatalytic mechanism and the photo-thermo-catalytic oxidation of volatile organic compounds under visible-light irradiation over $\text{Ag}_3\text{PO}_4/\text{Ag}/\text{SrTiO}_3$ is illustrated in Figure 8C, although electronic excitation of the STO suggests UV irradiation, as well as visible light irradiation. In this mechanism, the surface of Ag NP provide a selective route for the recombination of the photogenerated conduction

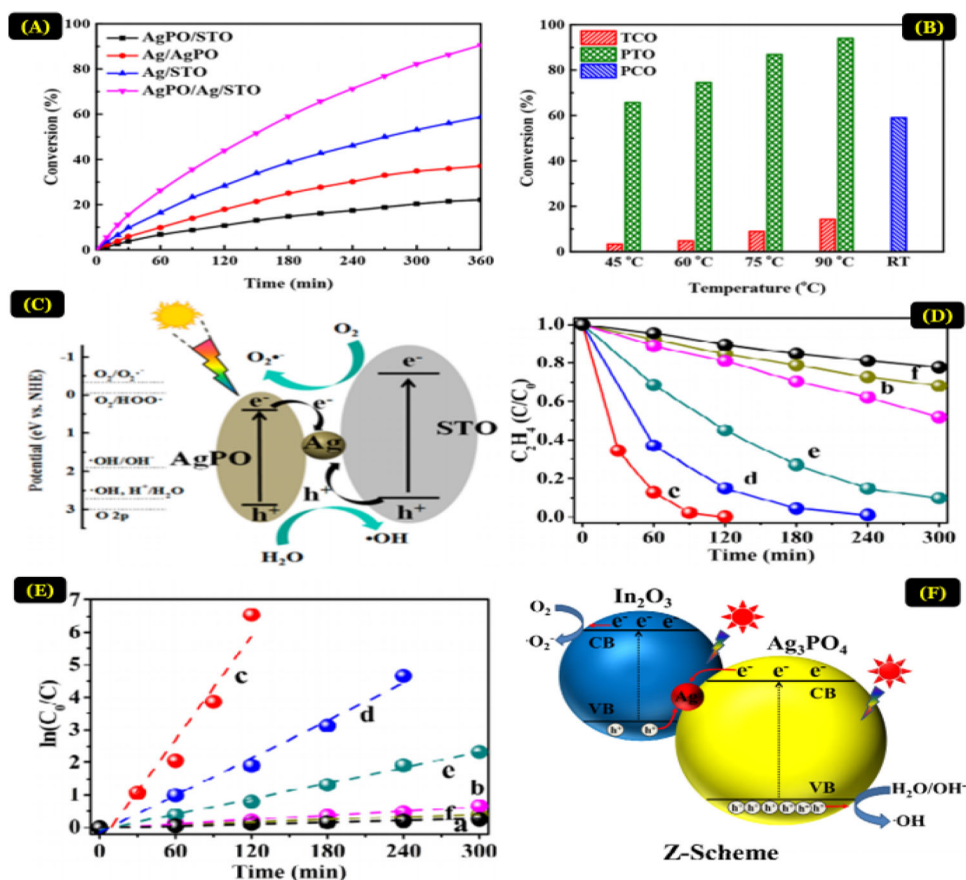


Figure 8. (A) Photocatalytic oxidation (PCO) of toluene under visible light at room temperature for 6 h; (B) Thermocatalytic oxidation (TCO), Photocatalytic oxidation (PCO), and photothermocatalytic oxidation (PTO) of toluene over $\text{Ag}_3\text{PO}_4/\text{Ag}/\text{SrTiO}_3$ for 3 h (RT refers to room temperature); (C) Charge transfer process in the photocatalytic oxidation process over $\text{Ag}_3\text{PO}_4/\text{Ag}/\text{SrTiO}_3$. (Figures 8A, 8B, and 8C are adapted with permission from ref. (Ji et al., 2019), copyright 2019 American Chemical Society); (D) Time courses of C_2H_4 photodegradation and (E) pseudo-first-order kinetics plots: a. In_2O_3 , 95-IO-Ag-5-AP, c. 90-IO-Ag-10-AP, d. 70-IO-Ag-30-AP, e. 50-IO-Ag-50-AP, f. Ag_3PO_4 ; (F) Charge transfer in the In_2O_3 -Ag- Ag_3PO_4 Z-scheme mode under sunlight illumination (Figures 8D, 8E, and 8F are adapted with permission from ref. (Chen et al., 2017), copyright 2017 Elsevier).

band electrons in Ag_3PO_4 and the photogenerated valence band holes in SrTiO_3 and in doing so help protect the Ag_3PO_4 photocatalyst from light corrosion (Ag^+ to Ag^0), thereby ensuring enhancement of $\text{Ag}_3\text{PO}_4/\text{Ag}/\text{SrTiO}_3$ photocatalytic stability.

5.4. Coupling Ag_3PO_4 with In_2O_3

In_2O_3 is an indirect band semiconductor with a direct bandgap of 3.6 eV and an indirect bandgap of 2.8 eV and regarded as an efficient

photocatalyst, as it increases the semiconductor absorption spectra from the UV region into the visible region (Liu et al., 2018; Mu et al., 2012; Yang et al., 2017). Recently, one group (Chen et al., 2017), has investigated the visible-light-driven oxidation of ethylene (C_2H_4) by O_2 photocatalysed by In_2O_3 -Ag- Ag_3PO_4 composites. These researchers found that the In_2O_3 -Ag- Ag_3PO_4 composite with 9:1 (90-IO-Ag-10-AP) mass ratio exhibited the highest rate for C_2H_4 photodegradation, decomposing almost 200 ppm C_2H_4 within 2 h under visible light irradiation (Figure 8D). Note, in this work, only the production of CO_2 was detected during the photocatalytic oxidation of C_2H_4 and the kinetics of the reaction were first order with respect to $[C_2H_4]$ (Figure 8E). The value of the first order rate constant for C_2H_4 removal determined for the 90-IO-Ag-10-AP photocatalyst was found to be 24.4 and 41.1 times higher than that determined for the In_2O_3 and Ag_3PO_4 photocatalysts, respectively. However, note that the degradation proficiency of the photocatalysts decreased after 3 reaction cycles.

A schematic diagram of reaction mechanism associated with the photocatalytic oxidation process driven by the photoexcited In_2O_3 -Ag- Ag_3PO_4 composite is illustrated in Figure 8F. Once again, in this mechanism, it is proposed that the photogenerated conduction band electrons on the Ag_3PO_4 particles combine with the photogenerated holes on the In_2O_3 , via the bridging Ag nanoparticles, thereby leading to the efficient separation of photo-generated charge carriers, which in turn slow down the Ag_3PO_4 photo-corrosion. Simultaneously, the efficient reduction of adsorbed O_2 over the In_2O_3 surface by its photogenerated conduction band electrons results in the production of reactive superoxide radical anions $\bullet O_2^-$, which eventually are reduced to water. At the same time the photogenerated valence band holes on the Ag_3PO_4 particles are able to effect the efficient oxidation of adsorbed water molecules or surface hydroxyl groups thereby producing hydroxyl radicals $\bullet OH$ which are able to oxidize the ethylene to CO_2 .

5.5. Coupling Ag_3PO_4 with $Sr_2Nb_2O_7$

$Sr_2Nb_2O_7$ is viewed currently as a most promising visible-light-driven photocatalyst, and has a low bandgap (3.9 eV) (Adhikari et al., 2018; Guo et al., 2014; Nisar et al., 2012). Thus, Guo et al. (Guo et al., 2014) have reported the preparation of different temperature based (873 K, 923 K, 973 K, 1023 K, 1073 K, and 1173 K), novel Ag_3PO_4 /nitridized $Sr_2Nb_2O_7$ (nitrided under NH_3 flow (500 mL min^{-1})) photocatalysts for the oxidation of IPA under visible light irradiation. Electronic structure calculations suggest that the valence band of $Sr_2Nb_2O_7$ might be significantly shifted (made less

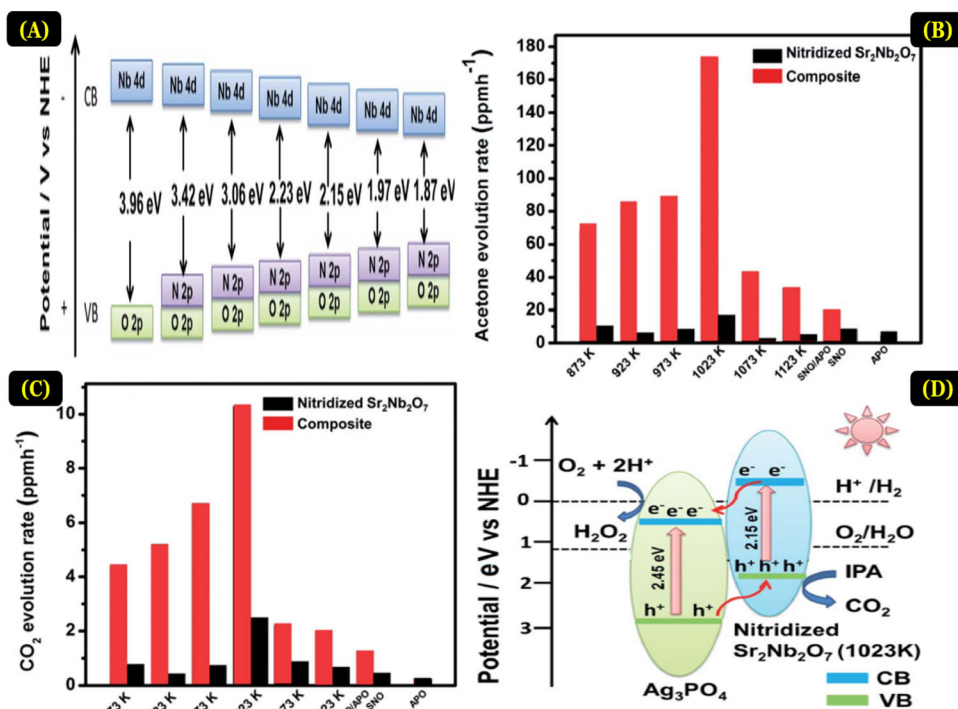


Figure 9. (A) The schematic band structures of nitridized $\text{Sr}_2\text{Nb}_2\text{O}_7$ (N: 0–6.18 wt%); (B) The acetone evolution rates of the as-prepared composite photocatalysts; (C) The CO_2 evolution rates of the as-prepared composite photocatalysts; (D) The schematic band structure of the $\text{Ag}_3\text{PO}_4/\text{SNON-1023}$ composite photocatalyst. Adapted with permission from ref. (Guo et al., 2014) Copyright 2014 Royal Society of Chemistry).

positive) with nitrogen doping (Figure 9A), which in turn suggests that the electronic structure of the $\text{Ag}_3\text{PO}_4/\text{nitridized Sr}_2\text{Nb}_2\text{O}_7$ photocatalysts can be altered by controlling the nitrogen dose in nitridized $\text{Sr}_2\text{Nb}_2\text{O}_7$. All the composite photocatalysts tested displayed superior photoactivity than the pristine materials, with the being a $\text{Ag}_3\text{PO}_4/\text{SNON-1023}$ photocatalyst which achieved maximum CO_2 and acetone evolution rates 10.32 ppm h^{-1} and 173.3 ppm h^{-1} , respectively (Figure 9B) and (Figure 9C). Other work showed that by increasing the nitridation temperature to 1023 K, the $\text{Ag}_3\text{PO}_4/\text{SNON-1023}$ increased in activity, as shown by the rate of photo-induced evolution of acetone (Figure 9B) and CO_2 (Figure 9C). However, above a nitridation temperature of 1023 K, increasing temperature resulted in a significant loss of activity. The observed variation in photocatalytic activity, illustrated in Figures 9B and C, is assumed to be due to the change in the valence band position of the nitridized $\text{Sr}_2\text{Nb}_2\text{O}_7$ (Figure 9D). The results of this work suggest that the optimal band gap of the nitridized $\text{Sr}_2\text{Nb}_2\text{O}_7$ is ca. 2.15 eV, with CB and VB potentials of -0.27 eV and $+1.88 \text{ eV}$, respectively. The results of this study indicate that the Ag_3PO_4

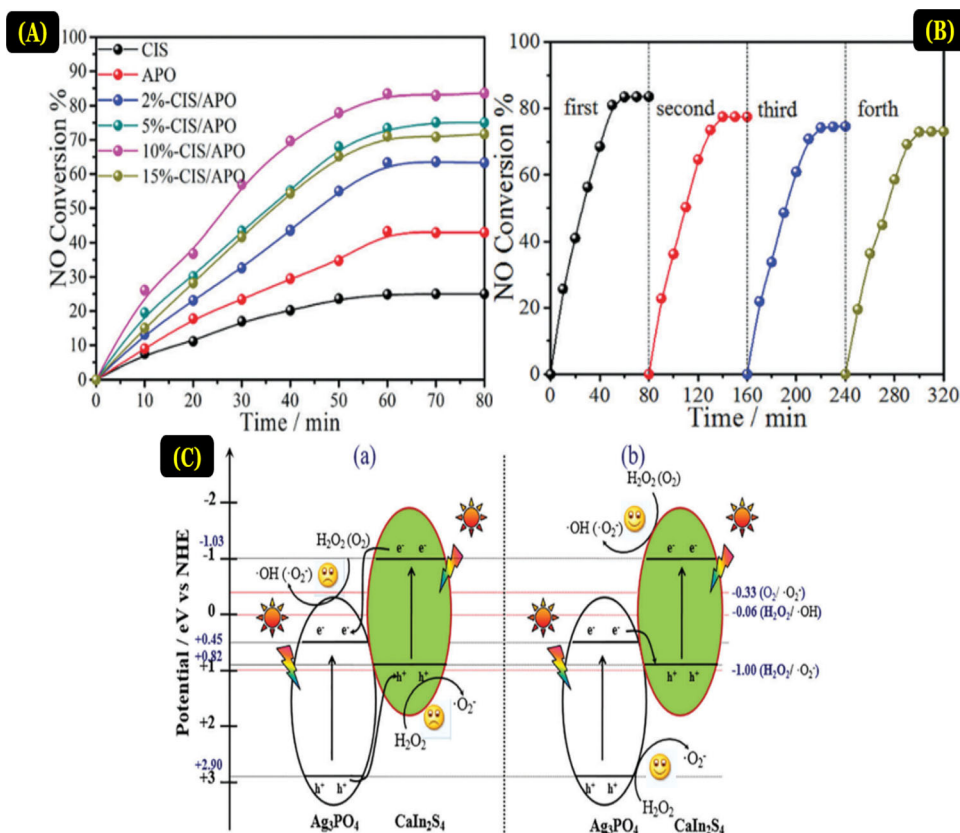


Figure 10. (A) The NO conversion efficiency of CIS, APO, and x%-CIS/APO nanocomposites ($x = 2, 5, 10, 15$); (B) the stability tests of the 10%-CIS/APO nanocomposite for NO removal. The schematic band structures of nitridized $\text{Sr}_2\text{Nb}_2\text{O}_7$ (N: 0–6.18 wt%); (C) Schematic representation of the photoexcited electron-hole transfer mechanism. Adapted with permission from ref. (Wan et al., 2018), copyright 2018 Royal Society of Chemistry).

valance and conduction bands potentials as well as those of the nitridized $\text{Sr}_2\text{Nb}_2\text{O}_7$ have an important effect on photoactivity.

5.6. Coupling Ag_3PO_4 with CaIn_2S_4

CaIn_2S_4 belongs to the AB_2X_4 semiconductor family which possesses suitable band edge positions (Li et al., 2017), high chemical stability (Liu et al., 2019), and narrow bandgaps (Wan et al., 2018), that in turn renders them very effective as photocatalysts (Ding et al., 2014; Jo & Natarajan, 2015; Li et al., 2017; Liu et al., 2019).

Wan et al. (2018), prepared a number of different Z-scheme $\text{CaIn}_2\text{S}_4/\text{Ag}_3\text{PO}_4$ nanocomposites (called CIS/APO) via wet impregnation method, and by changing the CaIn_2S_4 concentration from 0 to 15 wt%. These photocatalysts were then used to effect the photooxidation of nitric oxide (NO)

(~400 ppm) using a 300 W Xe-lamp as a solar light production source. The highest rate of NO oxidation was achieved using a $\text{CaIn}_2\text{S}_4/\text{Ag}_3\text{PO}_4$ photocatalyst with 10 wt% of CaIn_2S_4 (Figure 10A). Thus, the 10%-CIS/APO nanocomposite exhibited a 2-fold and 3.5-fold higher solar light-driven rate of photocatalytic oxidation of nitric oxide after 80 min irradiation than the pristine photocatalytic samples Ag_3PO_4 and CaIn_2S_4 , respectively (Figure 10A). The $\text{CaIn}_2\text{S}_4/\text{Ag}_3\text{PO}_4$ nanocomposite photocatalyst also exhibited high photostability over four photocatalytic oxidation of NO cycles (Figure 10B).

A schematic illustration of the major electron transfer processes associated with the above photocatalytic system is illustrated in Figure 10C. The results demonstrate that the coupling of CaIn_2S_4 and Ag_3PO_4 does not follow the conventional $\text{CaIn}_2\text{S}_4/\text{Ag}_3\text{PO}_4$ heterojunction (type II, see Figure 10Ca) because of the more positive potential of Ag_3PO_4 CB (+0.45 eV) (Krungchanuchat et al., 2017) than the produced $\bullet\text{O}_2^-$ and $\bullet\text{OH}$ formation ($\text{O}_2/\bullet\text{O}_2^- = -0.33$ eV; $\text{H}_2\text{O}_2/\bullet\text{OH} = +0.06$ eV) redox potential (Krungchanuchat et al., 2017), as well as the more negative potential of CaIn_2S_4 VB (+0.82 eV) (Wan et al., 2018) than the potential required for the oxidation of H_2O_2 to $\bullet\text{O}_2^-$ (+1.00 eV) (Krungchanuchat et al., 2017).

Instead, the coupling of CaIn_2S_4 and Ag_3PO_4 suggests Z-scheme mechanism (see Figure 10Cb), in which the photogenerated conduction band electrons on the Ag_3PO_4 conduction band recombine with the photogenerated valence band holes on the CaIn_2S_4 . As a result the remaining photogenerated holes on the Ag_3PO_4 are able to effect the production of OH radicals which are able to oxidize NO and the photogenerated conduction band electrons on the CaIn_2S_4 are able to effect the reduction of O_2 . As a result, the $\text{CaIn}_2\text{S}_4/\text{Ag}_3\text{PO}_4$ nanocomposite photocatalysts exhibit a higher efficiency for the oxidation of NO than the pristine CaIn_2S_4 or Ag_3PO_4 photocatalysts.

6. Conclusions and future directions

Silver phosphate is believed to be the most effective photocatalysts recorded to date since its first application in photocatalysis in 2009. Also, it is considered to be the most efficient visible-light-driven photocatalyst exhibiting remarkable photocatalytic properties than commonly employed oxidative photocatalysts such as TiO_2 , ZnO , BiVO_4 , and WO_3 . The only drawback for Ag_3PO_4 use as a photocatalyst is its photo-corrosion, which limits its potential in photocatalytic reactions. Consequently, many research efforts have been devoted to improving Ag_3PO_4 stability and its photocatalytic performance in environmental photo remediation studies. This review

reveals that its incorporation in a Z- scheme semiconductor heterojunction with other photocatalyst or into a more conventional type-II heterojunction could effectively enhance its stability and photocatalytic activity toward gaseous pollutants elimination. The enhanced photocatalytic oxidation of gaseous contaminants is closely associated with narrow bandgap energy, improved absorption light range, reduce electron-hole pair recombination, faster charge transfer, and negligible photo-corrosion.

Thus, this review's main purpose has been to compile the current research progress on the current strategies for enhancing Ag_3PO_4 -based composite photocatalytic activities toward gaseous pollutants elimination. Also, to discuss the proposed mechanisms responsible for the enhanced photocatalytic performance of the Ag_3PO_4 -based composite systems. Although considerable advances in this area have already been made over the past few years, most studies in this field are still at the initial stage. Thus, future work should focus on the following aspects:

- i. The use of Ag_3PO_4 -based composite photocatalysts should be extended toward the degradation of other harmful gases, such as acetaldehyde, trichloroethylene ... *etc.*
- ii. Photocatalyst synthetic methods that are more environmentally friendly and simpler should be investigated. Thus, systematic studies are needed urgently to introduce sustainable production pathways to provide a selection based material fabrication with the desired morphology, crystal phase, surface structure, as these characteristics strongly influence its photocatalytic activity.
- iii. The efficacy of core@shell structure photocatalysts based on Ag_3PO_4 -based composite semiconductors need to be investigated as they could effectively improve the photostability of the Ag_3PO_4 . This work would also provide a better understanding of the relationship between semiconductor photocatalyst structural properties and its photocatalytic performance.
- iv. In order to understand, the mechanism of the Ag_3PO_4 -based composite systems, different novel characterization and computational techniques, such as density functional theory (DFT), are required as they will be able to provide invaluable insights into the relationship between activity and material structural characteristics, such as i.e., surfaces, interfaces, nanostructures and activity at the atomic and molecular level.
- v. Bare Ag_3PO_4 showed a low surface area, which inhibits the kinetics and the photocatalytic degradation rate. Therefore, it is highly desirable to combine bare Ag_3PO_4 with adsorbing/porous surface materials such as activated carbon, graphene, lignocellulosic biomass, or clays in order to enhanced the available surface area and observed photoactivity.

- vi. The problems of scaling up these systems for operating under real conditions need to be addressed.

If the above issues and challenges are adequately addressed, then in years to come, the use of Ag_3PO_4 based Z-scheme or conventional type-II heterojunction photocatalysts for gaseous phase contaminants destruction is likely to be significant in air-pollution control.

Funding

This work was supported by the Ibn Zohr University (Morocco).

ORCID

M. Laabd  <http://orcid.org/0000-0001-7535-7299>

References

- Aarab, N., Hsini, A., Laabd, M., Essekre, A., Laktif, T., Haki, M. A., Lakhmiri, R., & Albourine, A. (2020). Theoretical study of the adsorption of sodium salicylate and metronidazole on the PANi. *Materials Today: Proceedings*, 22, 100–103. <https://doi.org/10.1016/j.matpr.2019.08.103>
- Abdellaoui, Y., Abou Oualid, H., Hsini, A., El Ibrahim, B., Laabd, M., El Ouardi, M., Giacomán-Vallejos, G., & Gamero-Melo, P. (2021). Synthesis of zirconium-modified Merlinoite from fly ash for enhanced removal of phosphate in aqueous medium: Experimental studies supported by Monte Carlo/SA simulations. *Chemical Engineering Journal and the Biochemical Engineering Journal.*, 404, 126600. <https://doi.org/10.1016/j.cej.2020.126600>
- Adhikari, S. P., Hood, Z. D., Chen, V. W., More, K. L., Senevirathne, K., & Lachgar, A. (2018). Visible-light-active g- C_3N_4 /N-doped $\text{Sr}_2\text{Nb}_2\text{O}_7$ heterojunctions as photocatalysts for the hydrogen evolution reaction. *Sustainable Energy & Fuels*, 2(11), 2507–2515. <https://doi.org/10.1039/C8SE00319J>
- Aghighi, A., & Haghghat, F. (2015). Using physical-chemical properties of reactants to estimate the performance of photocatalytic oxidation air cleaners. *Building and Environment.*, 85, 114–122. <https://doi.org/10.1016/j.buildenv.2014.11.020>
- Ait Ahsaine, H., Slassi, A., Naciri, Y., Chennah, A., Jaramillo-Páez, C., Anfar, Z., Zbair, M., Benlhachemi, A., & Navío, J. A. (2018). Photo/electrocatalytic properties of nanocrystalline ZnO and La-Doped ZnO: Combined DFT fundamental semiconducting properties and experimental study. *ChemistrySelect*, 3(27), 7778–7791. <https://doi.org/10.1002/slct.201801729>
- Ajmal, Z., Muhmood, A., Dong, R., & Wu, S. (2020). Probing the efficiency of magnetically modified biomass-derived biochar for effective phosphate removal. *Journal of Environmental Management*, 253, 109730. <https://doi.org/10.1016/j.jenvman.2019.109730>
- Ajmal, Z., Muhmood, A., Usman, M., Kizito, S., Lu, J., Dong, R., & Wu, S. (2018). Phosphate removal from aqueous solution using iron oxides: Adsorption, desorption and regeneration characteristics. *Journal of Colloid and Interface Science.*, 528, 145–155. <https://doi.org/10.1016/j.jcis.2018.05.084>

- Ajmal, Z., Usman, M., Anastopoulos, I., Qadeer, A., Zhu, R., Wakeel, A., & Dong, R. (2020). Use of nano-/micro-magnetite for abatement of cadmium and lead contamination. *Journal of environmental management*, 264, 110477. <https://doi.org/10.1016/j.jenvman.2020.110477>
- Amaterz, E., Tara, A., Bouddouch, A., Taoufyq, A., Bakiz, B., Benlhachemi, A., & Jbara, O. (2020). Photo-electrochemical degradation of wastewaters containing organics catalysed by phosphate-based materials: A review. *Reviews in Environmental Science and Biotechnology*, 19, 843–872. <https://doi.org/10.1007/s11157-020-09547-9>
- Amaterz, E., Tara, A., Bouddouch, A., Taoufyq, A., Bakiz, B., Lazar, F., Gilliot, M., Benlhachemi, A., Bazzi, L., & Jbara, O. (2020). Hierarchical flower-like SrHPO₄ electrodes for the photoelectrochemical degradation of Rhodamine B. *Journal of Applied Electrochemistry*, 50(5), 569–581. <https://doi.org/10.1007/s10800-020-01416-1>
- Amonette, J. E., & Matyáš, J. (2017). Functionalized silica aerogels for gas-phase purification, sensing, and catalysis: A review. *Microporous and Mesoporous Materials*, 250, 100–119. <https://doi.org/10.1016/j.micromeso.2017.04.055>
- Aramendía, M. A., Colmenares, J. C., Marinas, A., Marinas, J. M., Moreno, J. M., Navío, J. A., & Urbano, F. J. (2007). Effect of the redox treatment of Pt/TiO₂ system on its photocatalytic behaviour in the gas phase selective photooxidation of propan-2-ol. *Catalysis Today*, 128(3-4), 235–244. <https://doi.org/10.1016/j.cattod.2007.07.009>
- Araña, J., Alonso, A. P., Rodríguez, J. M. D., Colón, G., Navío, J. A., & Peña, J. P. (2009). FTIR study of photocatalytic degradation of 2-propanol in gas phase with different TiO₂ catalysts. *Applied Catalysis B: Environmental*, 89(1-2), 204–213. <https://doi.org/10.1016/j.apcatb.2008.11.027>
- Araña, J., Doña-Rodríguez, J. M., González-Díaz, O., Tello Rendón, E., Herrera Melián, J. A., Colón, G., Navío, J. A., & Pérez Peña, J. (2004). Gas-phase ethanol photocatalytic degradation study with TiO₂ doped with Fe, Pd and Cu. *Journal of Molecular Catalysis A: Chemical*, 215(1-2), 153–160. <https://doi.org/10.1016/j.molcata.2004.01.020>
- Ardizzone, S., Bianchi, C. L., Cappelletti, G., Gialanella, S., Pirola, C., & Ragaini, V. (2007). Tailored anatase/brookite nanocrystalline TiO₂. The optimal particle features for liquid-gas-phase photocatalytic reactions. *The Journal of Physical Chemistry C*, 111(35), 13222–13231. <https://doi.org/10.1021/jp0741096>
- Ardizzone, S., Bianchi, C. L., Cappelletti, G., Naldoni, A., & Pirola, C. (2008). Photocatalytic degradation of toluene in the gas phase: Relationship between surface species and catalyst features. *Environmental Science & Technology*, 42(17), 6671–6676. <https://doi.org/10.1021/es8009327>
- Azzouz, A., Kailasa, S. K., Lee, S. S., J. Rascón, A., Ballesteros, E., Zhang, M., & Kim, K. H. (2018). Review of nanomaterials as sorbents in solid-phase extraction for environmental samples. *TrAC Trends in Analytical Chemistry*, 108, 347–369. <https://doi.org/10.1016/j.trac.2018.08.009>
- Ba Mohammed, B., Hsini, A., Abdellaoui, Y., Abou Oualid, H., Laabd, M., El Ouardi, M., Ait Addi, A., Yamni, K., & Tijani, N. (2020). Fe-ZSM-5 zeolite for efficient removal of basic Fuchsin dye from aqueous solutions: Synthesis, characterization and adsorption process optimization using BBD-RSM modeling. *Journal of Environmental Chemical Engineering*, 8(5), 104419. <https://doi.org/10.1016/j.jece.2020.104419>
- Ballari, M. M., Hunger, M., Hüskén, G., & Brouwers, H. J. H. (2010). NO_x photocatalytic degradation employing concrete pavement containing titanium dioxide. *Applied Catalysis B: Environmental*, 95(3-4), 245–254. <https://doi.org/10.1016/j.apcatb.2010.01.002>

- Banerjee, S., Dionysiou, D. D., & Pillai, S. C. (2015). Self-cleaning applications of TiO₂ by photo-induced hydrophilicity and photocatalysis. *Applied Catalysis B: Environmental*, 176-177, 396-428. <https://doi.org/10.1016/j.apcatb.2015.03.058>
- Barea, E., Montoro, C., & Navarro, J. A. R. (2014). Toxic gas removal-metal-organic frameworks for the capture and degradation of toxic gases and vapours. *Chemical Society Reviews*, 43(16), 5419-5430. <https://doi.org/10.1039/c3cs60475f>
- Barebita, H., Naciri, Y., Ferraa, S., Nimour, A., & Guedira, T. (2020). Investigation of structural and photocatalytic behavior of Bi₁₃B_{1-2x}V_xP_xO_{20.95+2x} (0 ≤ x ≤ 0.5). *Solid State Sciences*, 108, 106389. <https://doi.org/10.1016/j.solidstatesciences.2020.106389>
- Belaissaoui, B., Le Moullec, Y., & Favre, E. (2016). Energy efficiency of a hybrid membrane/condensation process for VOC (Volatile Organic Compounds) recovery from air: A generic approach. *Energy*, 95, 291-302. <https://doi.org/10.1016/j.energy.2015.12.006>
- Benafqir, M., Hsini, A., Laabd, M., Laktif, T., Ait Addi, A., Albourine, A., & El Alem, N. (2020). Application of Density Functional Theory computation (DFT) and Process Capability Study for performance evaluation of Orthophosphate removal process using Polyaniline@Hematite-titaniferous sand composite (PANI@HTS) as a substrate. *Separation and Purification Technology*, 236, 116286. <https://doi.org/10.1016/j.seppur.2019.116286>
- Bianchi, C. L., Cerrato, G., Morandi, S., Di Michele, A., Djellabi, R., & Capucci, V. (2020). Sustainable photocatalytic porcelain grés slabs active under LED light for indoor depollution and bacteria reduction. In *Handbook of smart photocatalytic materials*. INC. <https://doi.org/10.1016/b978-0-12-819049-4.00008-8>
- Bianchi, C. L., Gatto, S., Pirola, C., Naldoni, A., Di Michele, A., Cerrato, G., Crocellà, V., & Capucci, V. (2014). Photocatalytic degradation of acetone, acetaldehyde and toluene in gas-phase: Comparison between nano and micro-sized TiO₂. *Applied Catalysis B: Environmental*, 146, 123-130. <https://doi.org/10.1016/j.apcatb.2013.02.047>
- Bianchi, C. L., Pirola, C., Stucchi, M., Sacchi, B., Cerrato, G., Morandi, S., Di Michele, A., Carletti, A., & Capucci, V. (2016). A new frontier of photocatalysis employing micro-sized TiO₂: Air/water pollution abatement and self-cleaning/antibacterial applications. *Semiconductor Photocatalytic - Material Mechanical Application*, 635-666. <https://doi.org/10.5772/62892>
- Bickley, R. I., Munuera, G., & Stone, F. S. (1973). Photoadsorption and photocatalysis at rutile surfaces. II. Photocatalytic oxidation of isopropanol. *Journal of Catalysis*, 31(3), 398-407. [https://doi.org/10.1016/0021-9517\(73\)90311-4](https://doi.org/10.1016/0021-9517(73)90311-4)
- Bierman, M. J., Lau, Y. K. A., Kvit, A. V., Schmitt, A. L., & Jin, S. (2008). Dislocation-driven nanowire growth and Eshelby twist. *Science (New York, N.Y.)*, 320(5879), 1060-1063. <https://doi.org/10.1126/science.1157131>
- Bouziani, A., Park, J., & Ozturk, A. (2020). Synthesis of α-Fe₂O₃/TiO₂ heterogeneous composites by the sol-gel process and their photocatalytic activity. *Journal of Photochemistry and Photobiology A: Chemistry*, 400, 112718. <https://doi.org/10.1016/j.jphotochem.2020.112718>
- Boyjoo, Y., Sun, H., Liu, J., Pareek, V. K., & Wang, S. (2017). A review on photocatalysis for air treatment: From catalyst development to reactor design. *Chemical Engineering Journal and the Biochemical Engineering Journal*, 310, 537-559. <https://doi.org/10.1016/j.cej.2016.06.090>
- Cai, T., Zeng, W., Liu, Y., Wang, L., Dong, W., Chen, H., & Xia, X. (2020). A promising inorganic-organic Z-scheme photocatalyst Ag₃PO₄/PDI supermolecule with enhanced photoactivity and photostability for environmental remediation. *Applied Catalysis B: Environmental*, 263, 118327. <https://doi.org/10.1016/j.apcatb.2019.118327>

- Cappelletti, G., Ardizzone, S., Bianchi, C. L., Gialanella, S., Naldoni, A., Pirola, C., & Ragaini, V. (2008). Photodegradation of pollutants in air: Enhanced properties of Nano-TiO₂ Prepared by ultrasound. *Nanoscale Research Letters*, 4(2), 97–105. <https://doi.org/10.1007/s11671-008-9208-3>
- Chai, Y., Ding, J., Wang, L., Liu, Q., Ren, J., & Dai, W. L. (2015). Enormous enhancement in photocatalytic performance of Ag₃PO₄/HAP composite: A Z-scheme mechanism insight. *Applied Catalysis B: Environmental*, 179, 29–36. <https://doi.org/10.1016/j.apcatb.2015.05.006>
- Che, H., Liu, C., Che, G., Liao, G., Dong, H., Li, C., Song, N., & Li, C. (2020). Facile construction of porous intramolecular g-C₃N₄-based donor-acceptor conjugated copolymers as highly efficient photocatalysts for superior H₂ evolution. *Nano Energy*, 67, 104273. <https://doi.org/10.1016/j.nanoen.2019.104273>
- Chen, X., Huang, X., & Yi, Z. (2014). Enhanced ethylene photodegradation performance of g-C₃N₄-Ag₃PO₄ composites with direct Z-scheme configuration. *Chemistry (Weinheim an Der Bergstrasse, Germany)*, 20(52), 17590–17596. <https://doi.org/10.1002/chem.201404284>
- Chen, X., Li, R., Pan, X., Huang, X., & Yi, Z. (2017). Fabrication of In₂O₃-Ag-Ag₃PO₄ composites with Z-scheme configuration for photocatalytic ethylene degradation under visible light irradiation. *Chemical Engineering Journal and the Biochemical Engineering Journal.*, 320, 644–652. <https://doi.org/10.1016/j.cej.2017.03.072>
- Chen, Z., Bing, F., Liu, Q., Zhang, Z., & Fang, X. (2015). Novel Z-scheme visible-light-driven Ag₃PO₄/Ag/SiC photocatalysts with enhanced photocatalytic activity. *Journal of Materials Chemistry A*, 3(8), 4652–4658. <https://doi.org/10.1039/C4TA06530A>
- Chen, Z., Wang, W., Zhang, Z., & Fang, X. (2013). High-efficiency visible-light-driven Ag₃PO₄/AgI photocatalysts: Z - Scheme photocatalytic mechanism for their enhanced photocatalytic activity. *The Journal of Physical Chemistry C*, 117(38), 19346–19352. <https://doi.org/10.1021/jp406508y>
- Chenchana, A., Nemancha, A., Moumeni, H., Doña Rodríguez, J. M., Araña, J., Navío, J. A., González Díaz, O., & Pulido Melián, E. (2019). Photodegradation of 2,4-dichlorophenoxyacetic acid over TiO₂ (B)/anatase nanobelts and Au-TiO₂ (B)/anatase nanobelts. *Applied Surface Science.*, 467-468, 1076–1087. <https://doi.org/10.1016/j.apsusc.2018.10.175>
- Cho, H. (2017). An air quality and event detection system with life logging for monitoring household environments. *Smart Sensors IoT Front*, 2, 251–270. https://doi.org/10.1007/978-3-319-55345-0_10
- da Costa Filho, B. M., Araujo, A. L. P., Padrão, S. P., Boaventura, R. A. R., Dias, M. M., Lopes, J. C. B., & Vilar, V. J. P. (2019). Effect of catalyst coated surface, illumination mechanism and light source in heterogeneous TiO₂ photocatalysis using a mili-photo-reactor for n-decane oxidation at gas phase. *Chemical Engineering Journal and the Biochemical Engineering Journal*, 366, 560–568. <https://doi.org/10.1016/j.cej.2019.02.122>
- da Costa Filho, B. M., Araujo, A. L. P., Silva, G. V., Boaventura, R. A. R., Dias, M. M., Lopes, J. C. B., & Vilar, V. J. P. (2017). Intensification of heterogeneous TiO₂ photocatalysis using an innovative micro-meso-structured-photo-reactor for n-decane oxidation at gas phase. *Chemical Engineering Journal and the Biochemical Engineering Journal*, 310, 331–341. <https://doi.org/10.1016/j.cej.2016.09.080>
- da Costa Filho, B. M., Silva, G. V., Boaventura, R. A. R., Dias, M. M., Lopes, J. C. B., & Vilar, V. J. P. (2019). Ozonation and ozone-enhanced photocatalysis for VOC removal from air streams: Process optimization, synergy and mechanism assessment. *The Science of the Total Environment*, 687, 1357–1368. <https://doi.org/10.1016/j.scitotenv.2019.05.365>

- da Costa Filho, B. M., & Vilar, V. J. P. (2020). Strategies for the intensification of photocatalytic oxidation processes towards air streams decontamination: A review. *Chemical Engineering Journal and the Biochemical Engineering Journal*, 391, 123531. <https://doi.org/10.1016/j.cej.2019.123531>
- Deng, X., Chen, Y., Wen, J., Xu, Y., Zhu, J., & Bian, Z. (2020). Polyaniline-TiO₂ composite photocatalysts for light-driven hexavalent chromium ions reduction. *Science Bulletin*, 65(2), 105–112. <https://doi.org/10.1016/j.scib.2019.10.020>
- Ding, J., Hong, B., Luo, Z., Sun, S., Bao, J., & Gao, C. (2014). Mesoporous monoclinic CaIn₂S₄ with surface nanostructure: An efficient photocatalyst for hydrogen production under visible light. *The Journal of Physical Chemistry C*, 118(48), 27690–27697. <https://doi.org/10.1021/jp508497a>
- Djaghri, N., Formenti, M., Juillet, F., & Teichner, S. J. (1974). Photointeraction on the surface of titanium dioxide between oxygen and alkanes. *Faraday Discussions of the Chemical Society*, 58, 185–193. <https://doi.org/10.1039/dc9745800185>
- Djellabi, R., Fouzi Ghorab, M., Smara, A., Bianchi, C. L., Cerrato, G., Zhao, X., & Yang, B. (2020). Titania–montmorillonite for the photocatalytic removal of contaminants from water: Adsorb & shuttle process. *Green Material Wastewater Treatment*, 38, 291–319. https://doi.org/10.1007/978-3-030-17724-9_13
- Djellabi, R., Yang, B., Adeel Sharif, H. M., Zhang, J., Ali, J., & Zhao, X. (2019). Sustainable and easy recoverable magnetic TiO₂-Lignocellulosic Biomass@Fe₃O₄ for solar photocatalytic water remediation. *Journal of Cleaner Production*, 233, 841–847. <https://doi.org/10.1016/j.jclepro.2019.06.125>
- Djellabi, R., Yang, B., Xiao, K., Gong, Y., Cao, D., Sharif, H. M. A., Zhao, X., Zhu, C., & Zhang, J. (2019). Unravelling the mechanistic role of TiOC bonding bridge at titania/lignocellulosic biomass interface for Cr(VI) photoreduction under visible light. *Journal of Colloid and Interface Science*, 553, 409–417. <https://doi.org/10.1016/j.jcis.2019.06.052>
- Dong, G., Zhang, Y., Pan, Q., & Qiu, J. (2014). A fantastic graphitic carbon nitride (g-C₃N₄) material: Electronic structure, photocatalytic and photoelectronic properties. *Journal of Photochemistry and Photobiology C: Photochemistry Reviews*, 20, 33–50. <https://doi.org/10.1016/j.jphotochemrev.2014.04.002>
- Dong, P., Hou, G., Liu, C., Zhang, X., Tian, H., Xu, F., Xi, X., & Shao, R. (2016). Origin of activity and stability enhancement for Ag₃PO₄ photocatalyst after calcination. *Materials (Basel)*, 9(12), 968–917. <https://doi.org/10.3390/ma9120968>
- Ehn, M., Thornton, J. A., Kleist, E., Sipilä, M., Junninen, H., Pullinen, I., Springer, M., Rubach, F., Tillmann, R., Lee, B., Lopez-Hilfiker, F., Andres, S., Acir, I. H., Rissanen, M., Jokinen, T., Schobesberger, S., Kangasluoma, J., Kontkanen, J., Nieminen, T., ... Mentel, T. F. (2014). A large source of low-volatility secondary organic aerosol. *Nature*, 506(7489), 476–479. <https://doi.org/10.1038/nature13032>
- Erdogan, N., Bouziani, A., Park, J., Micusik, M., Kim, S. Y., Majkova, E., Omastova, M., & Ozturk, A. (2019). Synthesis and enhanced photocatalytic activity of nitrogen-doped triphasic TiO₂ nanoparticles. *Journal of Photochemistry and Photobiology A: Chemistry*, 377, 92–100. <https://doi.org/10.1016/j.jphotochem.2019.03.047>
- Essekri, A., Hsini, A., Naciri, Y., Laabd, M., Ajmal, Z., El Ouardi, M., Ait Addi, A., & Albourine, A. (2020). Novel citric acid-functionalized brown algae with a high removal efficiency of crystal violet dye from colored wastewaters: Insights into equilibrium, adsorption mechanism, and reusability. *International Journal of Phytoremediation*, 0, 1–11. <https://doi.org/10.1080/15226514.2020.1813686>

- Farhanian, D., Haghighat, F., Lee, C. S., & Lakdawala, N. (2013). Impact of design parameters on the performance of ultraviolet photocatalytic oxidation air cleaner. *Building and Environment*, 66, 148–157. <https://doi.org/10.1016/j.buildenv.2013.04.010>
- Fino, D., Bensaid, S., Piumetti, M., & Russo, N. (2016). A review on the catalytic combustion of soot in Diesel particulate filters for automotive applications: From powder catalysts to structured reactors. *Applied Catalysis A: General*, 509, 75–96. <https://doi.org/10.1016/j.apcata.2015.10.016>
- Fiorenza, R., Di Mauro, A., Cantarella, M., Iaria, C., Scalisi, E. M., Brundo, M. V., Gulino, A., Spitaleri, L., Nicotra, G., Dattilo, S., Carroccio, S. C., Privitera, V., & Impellizzeri, G. (2020). Preferential removal of pesticides from water by molecular imprinting on TiO₂ photocatalysts. *Chemical Engineering Journal and the Biochemical Engineering Journal*, 379, 122309. <https://doi.org/10.1016/j.cej.2019.122309>
- Ganesh, V. A., Raut, H. K., Nair, A. S., & Ramakrishna, S. (2011). A review on self-cleaning coatings. *Journal of Materials Chemistry*, 21(41), 16304–16322. <https://doi.org/10.1039/c1jm12523k>
- Ge, M., Zhu, N., Zhao, Y., Li, J., & Liu, L. (2012). Sunlight-assisted degradation of dye pollutants in Ag₃PO₄ suspension. *Industrial & Engineering Chemistry Research*, 51(14), 5167–5173. <https://doi.org/10.1021/ie202864n>
- Guo, J., Ouyang, S., Li, P., Zhang, Y., Kako, T., & Ye, J. (2013). A new heterojunction Ag₃PO₄/Cr-SrTiO₃ photocatalyst towards efficient elimination of gaseous organic pollutants under visible light irradiation. *Applied Catalysis B: Environmental*, 134–135, 286–292. <https://doi.org/10.1016/j.apcatb.2012.12.038>
- Guo, J., Zhou, H., Ouyang, S., Kako, T., & Ye, J. (2014). An Ag₃PO₄/nitridized Sr₂Nb₂O₇ composite photocatalyst with adjustable band structures for efficient elimination of gaseous organic pollutants under visible light irradiation. *Nanoscale*, 6(13), 7303–7311. <https://doi.org/10.1039/c4nr00537f>
- Guo, T., Bai, Z., Wu, C., & Zhu, T. (2008). Influence of relative humidity on the photocatalytic oxidation (PCO) of toluene by TiO₂ loaded on activated carbon fibers: PCO rate and intermediates accumulation. *Applied Catalysis B: Environmental*, 79(2), 171–178. <https://doi.org/10.1016/j.apcatb.2007.09.033>
- He, F., Wang, Z., Li, Y., Peng, S., & Liu, B. (2020). The nonmetal modulation of composition and morphology of g-C₃N₄-based photocatalysts. *Applied Catalysis B: Environmental*, 269, 118828. <https://doi.org/10.1016/j.apcatb.2020.118828>
- He, R., Xu, D., Cheng, B., Yu, J., & Ho, W. (2018). Review on nanoscale Bi-based photocatalysts. *Nanoscale Horizons*, 3(5), 464–504. <https://doi.org/10.1039/c8nh00062j>
- Hsini, A., Essekre, A., Aarab, N., Laabd, M., Addi, A. A., Lakhmiri, R., & Albourine, A. (2020). Elaboration of novel polyaniline@Almond shell biocomposite for effective removal of hexavalent chromium ions and Orange G dye from aqueous solutions. *Environmental Science and Pollution Research*, 27, 15245–15258. <https://doi.org/10.1007/s11356-020-08039-1>
- Hsini, A., Naciri, Y., Benafqir, M., Ajmal, Z., Aarab, N., Laabd, M., Navío, J. A., Puga, F., Boukherroub, R., Bakiz, B., & Albourine, A. (2021). Facile synthesis and characterization of a novel 1,2,4,5-benzene tetracarboxylic acid doped polyaniline@zinc phosphate nanocomposite for highly efficient removal of hazardous hexavalent chromium ions from water. *Journal of Colloid and Interface Science*, 585, 560–573. <https://doi.org/10.1016/j.jcis.2020.10.036>
- Hsini, A., Naciri, Y., Laabd, M., El Ouardi, M., Ajmal, Z., Lakhmiri, R., Boukherroub, R., & Albourine, A. (2020). Synthesis and characterization of arginine-doped polyaniline/walnut shell hybrid composite with superior clean-up ability for chromium (VI) from

- aqueous media: Equilibrium, reusability and process optimization. *Journal of Molecular Liquids*, 316, 113832. <https://doi.org/10.1016/j.molliq.2020.113832>
- Huang, D., Chen, S., Zeng, G., Gong, X., Zhou, C., Cheng, M., Xue, W., Yan, X., & Li, J. (2019). Artificial Z-scheme photocatalytic system: What have been done and where to go? *Coordination Chemistry Reviews*, 385, 44–80. <https://doi.org/10.1016/j.ccr.2018.12.013>
- Jafarikojour, M., Sohrabi, M., Royae, S. J., & Hassanvand, A. (2015). Evaluation and optimization of a novel immobilized photoreactor for the degradation of gaseous toluene. *CLEAN - Soil, Air, Water*, 43(5), 662–670. <https://doi.org/10.1002/clen.201300985>
- Ji, W., Rui, Z., & Ji, H. (2019). Z-scheme $\text{Ag}_3\text{PO}_4/\text{Ag}/\text{SrTiO}_3$ heterojunction for visible-light induced photothermal synergistic VOCs degradation with enhanced performance. *Industrial & Engineering Chemistry Research*, 58(31), 13950–13959. <https://doi.org/10.1021/acs.iecr.9b02176>
- Jia, Y., Ma, Y., Zhu, L., Dong, J., & Lin, Y. (2019). Efficient visible-light-responsive photocatalyst: Hybrid $\text{TiO}_2\text{-Ag}_3\text{PO}_4$ nanorods. *Chemical Physics*, 521, 1–4. <https://doi.org/10.1016/j.chemphys.2019.01.015>
- Jo, W.-K., & Natarajan, T. S. (2015). Facile synthesis of novel redox-mediator-free direct Z-scheme CaIn_2S_4 marigold-flower-like/ TiO_2 photocatalysts with superior photocatalytic efficiency. *ACS Applied Materials & Interfaces*, 7(31), 17138–17154. <https://doi.org/10.1021/acsami.5b03935>
- Jo, W. K., & Kim, J. T. (2009). Application of visible-light photocatalysis with nitrogen-doped or unmodified titanium dioxide for control of indoor-level volatile organic compounds. *Journal of Hazardous Materials*, 164(1), 360–366. <https://doi.org/10.1016/j.jhazmat.2008.08.033>
- Jo, W. K., & Yang, C. H. (2009). Granular-activated carbon adsorption followed by annular-type photocatalytic system for control of indoor aromatic compounds. *Separation and Purification Technology*, 66(3), 438–442. <https://doi.org/10.1016/j.seppur.2009.02.014>
- Kahk, J. M., Sheridan, D. L., Kehoe, A. B., Scanlon, D. O., Morgan, B. J., Watson, G. W., & Payne, D. J. (2014). The electronic structure of silver orthophosphate: Experiment and theory. *Journal of Materials Chemistry A*, 2(17), 6092–6099. <https://doi.org/10.1039/C3TA14191H>
- Kamal, M. S., Razzak, S. A., & Hossain, M. M. (2016). Catalytic oxidation of volatile organic compounds (VOCs) - A review. *Atmospheric Environment*, 140, 117–134. <https://doi.org/10.1016/j.atmosenv.2016.05.031>
- Karafas, E. S., Romanias, M. N., Stefanopoulos, V., Binas, V., Zachopoulos, A., Kiriakidis, G., & Papagiannakopoulos, P. (2019). Effect of metal doped and co-doped TiO_2 photocatalysts oriented to degrade indoor/outdoor pollutants for air quality improvement. A kinetic and product study using acetaldehyde as probe molecule. *Journal of Photochemistry and Photobiology A: Chemistry*, 371, 255–263. <https://doi.org/10.1016/j.jphotochem.2018.11.023>
- Kong, J., Rui, Z., & Ji, H. (2016). Enhanced photocatalytic mineralization of gaseous toluene over SrTiO_3 by surface hydroxylation. *Industrial & Engineering Chemistry Research*, 55(46), 11923–11930. <https://doi.org/10.1021/acs.iecr.6b03270>
- Korologos, C. A., Philippopoulos, C. J., & Pouloupoulos, S. G. (2011). The effect of water presence on the photocatalytic oxidation of benzene, toluene, ethylbenzene and m-xylene in the gas-phase. *Atmospheric Environment*, 45(39), 7089–7095. <https://doi.org/10.1016/j.atmosenv.2011.09.038>
- Krishnamurthy, A., Adebayo, B., Gelles, T., Rownaghi, A., & Rezaei, F. (2019). Abatement of gaseous volatile organic compounds: A process perspective. *Catalysis Today*, 350, 100–119. <https://doi.org/10.1016/j.cattod.2019.05.069>

- Krungchanuchat, S., Ekthammathat, N., Phuruangrat, A., Thongtem, S., & Thongtem, T. (2017). High UV-visible photocatalytic activity of Ag_3PO_4 dodecahedral particles synthesized by a simple hydrothermal method. *Materials Letters*, 201, 58–61. <https://doi.org/10.1016/j.matlet.2017.04.131>
- Lam, S. M., Sin, J. C., Abdullah, A. Z., & Mohamed, A. R. (2012). Degradation of wastewaters containing organic dyes photocatalysed by zinc oxide: A review. *Desalination and Water Treatment*, 41(1-3), 131–169. <https://doi.org/10.1080/19443994.2012.664698>
- Li, G., Wang, Y., & Mao, L. (2014). Recent progress in highly efficient Ag-based visible-light photocatalysts. *RSC Advances*, 4(96), 53649–53661. <https://doi.org/10.1039/C4RA08044K>
- Li, J., Fang, W., Yu, C., Zhou, W., Zhu, L., & Xie, Y. (2015). Ag-based semiconductor photocatalysts in environmental purification. *Applied Surface Science*, 358, 46–56. <https://doi.org/10.1016/j.apsusc.2015.07.139>
- Li, J., Meng, S., Wang, T., Xu, Q., Shao, L., Jiang, D., & Chen, M. (2017). Novel Au/CaIn₂S₄ nanocomposites with plasmon-enhanced photocatalytic performance under visible light irradiation. *Applied Surface Science*, 396, 430–437. <https://doi.org/10.1016/j.apsusc.2016.10.172>
- Li, X., Zhang, L., Yang, Z., Wang, P., Yan, Y., & Ran, J. (2020). Adsorption materials for volatile organic compounds (VOCs) and the key factors for VOCs adsorption process: A review. *Separation and Purification Technology*, 235, 116213. <https://doi.org/10.1016/j.seppur.2019.116213>
- Li, X., Zhang, Z., Yao, C., Lu, X., Zhao, X., & Ni, C. (2016). Attapulgite-CeO₂/MoS₂ ternary nanocomposite for photocatalytic oxidative desulfurization. *Applied Surface Science*, 364, 589–596. <https://doi.org/10.1016/j.apsusc.2015.12.196>
- Liang, S., Zhang, D., Pu, X., Yao, X., Han, R., Yin, J., & Ren, X. (2019). A novel Ag₂O/g-C₃N₄ p-n heterojunction photocatalysts with enhanced visible and near-infrared light activity. *Separation and Purification Technology*, 210, 786–797. <https://doi.org/10.1016/j.seppur.2018.09.008>
- Liao, L., Heylen, S., Sree, S. P., Vallaey, B., Keulemans, M., Lenaerts, S., Roeffaers, M. B. J., & Martens, J. A. (2017). Photocatalysis assisted simultaneous carbon oxidation and NO_x reduction. *Applied Catalysis B: Environmental*, 202, 381–387. <https://doi.org/10.1016/j.apcatb.2016.09.042>
- Likodimos, V. (2018). Photonic crystal-assisted visible light activated TiO₂ photocatalysis. *Applied Catalysis B: Environmental*, 230, 269–303. <https://doi.org/10.1016/j.apcatb.2018.02.039>
- Liu, B., Liu, X., Li, L., Zhuge, Z., Li, Y., Li, C., Gong, Y., Niu, L., Xu, S., & Sun, C. Q. (2019). CaIn₂S₄ decorated WS₂ hybrid for efficient Cr(VI) reduction. *Applied Surface Science*, 484, 300–306. <https://doi.org/10.1016/j.apsusc.2019.03.322>
- Liu, J. J., Fu, X. L., Chen, S. F., & Zhu, Y. F. (2011). Electronic structure and optical properties of Ag₃PO₄ photocatalyst calculated by hybrid density functional method. *Applied Physics Letters*, 99(19), 191903–192014. <https://doi.org/10.1063/1.3660319>
- Liu, W. T., Wu, B. H., Lai, Y. T., Tai, N. H., Perng, T. P., & Chen, L. J. (2018). Enhancement of water splitting by controlling the amount of vacancies with varying vacuum level in the synthesis system of SnO_{2-x}/In₂O_{3-y} heterostructure as photocatalyst. *Nano Energy*, 47, 18–25. <https://doi.org/10.1016/j.nanoen.2018.02.037>
- Liu, Y., Kong, J., Yuan, J., Zhao, W., Zhu, X., Sun, C., & Xie, J. (2018). Enhanced photocatalytic activity over flower-like sphere Ag/Ag₂CO₃/BiVO₄ plasmonic heterojunction photocatalyst for tetracycline degradation. *Chemical Engineering Journal and the Biochemical Engineering Journal*, 331, 242–254. <https://doi.org/10.1016/j.cej.2017.08.114>

- Lopes, F. V. S., Monteiro, R. A. R., Silva, A. M. T., Silva, G. V., Faria, J. L., Mendes, A. M., Vilar, V. J. P., & Boaventura, R. A. R. (2012). Insights into UV-TiO₂ photocatalytic degradation of PCE for air decontamination systems. *Chemical Engineering Journal and the Biochemical Engineering Journal*, 204-206–(205), 244–257. <https://doi.org/10.1016/j.cej.2012.07.079>
- Low, J., Jiang, C., Cheng, B., Wageh, S., Al-Ghamdi, A. A., & Yu, J. (2017). A Review of Direct Z-Scheme Photocatalysts. *Small Methods*, 1(5), 1700080. <https://doi.org/10.1002/smt.201700080>
- Lu, B., Ma, N., Wang, Y., Qiu, Y., Hu, H., Zhao, J., Liang, D., Xu, S., Li, X., Zhu, Z., & Cui, C. (2015). Visible-light-driven TiO₂/Ag₃PO₄/GO heterostructure photocatalyst with dual-channel for photo-generated charges separation. *Journal of Alloys and Compounds*, 630, 163–171. <https://doi.org/10.1016/j.jallcom.2015.01.008>
- Luengas, A., Barona, A., Hort, C., Gallastegui, G., Platel, V., & Elias, A. (2015). A review of indoor air treatment technologies. *Reviews in Environmental Science and Bio/Technology*, 14(3), 499–522. <https://doi.org/10.1007/s11157-015-9363-9>
- Ma, X., Lu, B., Li, D., Shi, R., Pan, C., & Zhu, Y. (2011). Origin of photocatalytic activation of silver orthophosphate from first-principles. *The Journal of Physical Chemistry C*, 115(11), 4680–4687. <https://doi.org/10.1021/jp111167u>
- Malakar, S., Saha, P., Das, Baskaran, D., & Rajamanickam, R. (2017). Comparative study of biofiltration process for treatment of VOCs emission from petroleum refinery wastewater—A review. *Environmental Technology & Innovation*, 8, 441–461. <https://doi.org/10.1016/j.eti.2017.09.007>
- Mamaghani, A. H., Haghghat, F., & Lee, C. S. (2017). Photocatalytic oxidation technology for indoor environment air purification: The state-of-the-art. *Applied Catalysis B: Environmental*, 203, 247–269. <https://doi.org/10.1016/j.apcatb.2016.10.037>
- Martín-Gómez, A. N., Navío, J. A., Jaramillo-Páez, C., Sánchez-Cid, P., & Hidalgo, M. C. (2020). Hybrid ZnO/Ag₃PO₄ photocatalysts, with low and high phosphate molar percentages. *Journal of Photochemistry and Photobiology A: Chemistry*, 388, 112196. <https://doi.org/10.1016/j.jphotochem.2019.112196>
- Martin, D. J., Liu, G., Moniz, S. J. A., Bi, Y., Beale, A. M., Ye, J., & Tang, J. (2015). Efficient visible driven photocatalyst, silver phosphate: Performance, understanding and perspective. *Chemical Society Reviews*, 44(21), 7808–7828. <https://doi.org/10.1039/c5cs00380f>
- Masih, D., Ma, Y., & Rohani, S. (2017). Graphitic C₃N₄ based noble-metal-free photocatalyst systems: A review. *Applied Catalysis B: Environmental*, 206, 556–588. <https://doi.org/10.1016/j.apcatb.2017.01.061>
- Mazierski, P., Mikolajczyk, A., Bajorowicz, B., Malankowska, A., Zaleska-Medynska, A., & Nadolna, J. (2018). The role of lanthanides in TiO₂-based photocatalysis: A review. *Applied Catalysis B: Environmental*, 233, 301–317. <https://doi.org/10.1016/j.apcatb.2018.04.019>
- Monteiro, R. A. R., Miranda, S. M., Rodrigues-Silva, C., Faria, J. L., Silva, A. M. T., Boaventura, R. A. R., & Vilar, V. J. P. (2015). Gas phase oxidation of n-decane and PCE by photocatalysis using an annular photoreactor packed with a monolithic catalytic bed coated with P25 and PC500. *Applied Catalysis B: Environmental*, 165, 306–315. <https://doi.org/10.1016/j.apcatb.2014.10.026>
- Mu, J., Chen, B., Zhang, M., Guo, Z., Zhang, P., Zhang, Z., Sun, Y., Shao, C., & Liu, Y. (2012). Enhancement of the visible-light photocatalytic activity of In₂O₃-TiO₂ nanofiber heteroarchitectures. *ACS Applied Materials & Interfaces*, 4(1), 424–430. <https://doi.org/10.1021/am201499r>

- Murcia, J. J., Hidalgo, M. C., Navío, J. A., Vaiano, V., Ciambelli, P., & Sannino, D. (2012). Ethanol partial photooxidation on Pt/TiO₂ catalysts as green route for acetaldehyde synthesis. *Catalysis Today*, 196(1), 101–109. <https://doi.org/10.1016/j.cattod.2012.02.033>
- Naciri, Y., Ait Ahsaine, H., Chennah, A., Amedlous, A., Taoufyq, A., Bakiz, B., Ezahri, M., Villain, S., & Benlhachemi, A. (2018). Facile synthesis, characterization and photocatalytic performance of Zn₃(PO₄)₂ platelets toward photodegradation of Rhodamine B dye. *Journal of Environmental Chemical Engineering*, 6(2), 1840–1847. <https://doi.org/10.1016/j.jece.2018.02.009>
- Naciri, Y., Bouddouch, A., Bakiz, B., Taoufyq, A., Ezahri, M., & Benlhachemi, A. (2019). Photocatalytic degradation of sulfadiazine by Zn₃(PO₄)₂/BiPO₄ composites upon UV light irradiation. *Materials Today: Proceedings*, 3, 8–11. <https://doi.org/10.1016/j.matpr.2019.08.071>
- Naciri, Y., Chennah, A., Jaramillo-Páez, C., Navío, J. A., Bakiz, B., Taoufyq, A., Ezahri, M., Villain, S., Guinneton, F., & Benlhachemi, A. (2019). Preparation, characterization and photocatalytic degradation of Rhodamine B dye over a novel Zn₃(PO₄)₂/BiPO₄ catalyst. *Journal of Environmental Chemical Engineering*, 7(3), 103075. <https://doi.org/10.1016/j.jece.2019.103075>
- Naciri, Y., Hsini, A., Ajmal, Z., Bouddouch, A., Bakiz, B., Navío, J. A., Albourine, A., Valmalette, J. C., Ezahri, M., & Benlhachemi, A. (2020). Influence of Sr-doping on structural, optical and photocatalytic properties of synthesized Ca₃(PO₄)₂. *Journal of Colloid and Interface Science*, 572, 269–280. <https://doi.org/10.1016/j.jcis.2020.03.105>
- Naciri, Y., Hsini, A., Ajmal, Z., Navío, J. A., Bakiz, B., Albourine, A., Ezahri, M., & Benlhachemi, A. (2020). Recent progress on the enhancement of photocatalytic properties of BiPO₄ using π -conjugated materials. *Advances in Colloid and Interface Science*, 280, 102160. <https://doi.org/10.1016/j.cis.2020.102160>
- Navakoteswara Rao, V., Lakshmana Reddy, N., Mamatha Kumari, M., Ravi, P., Sathish, M., Kuruvilla, K. M., Preethi, V., Reddy, K. R., Shetti, N. P., Aminabhavi, T. M., & Shankar, M. V. (2019). Photocatalytic recovery of H₂ from H₂S containing wastewater: Surface and interface control of photo-excited in Cu₂S@TiO₂ core-shell nanostructures. *Applied Catalysis B: Environmental*, 254, 174–185. <https://doi.org/10.1016/j.apcatb.2019.04.090>
- Ng, H. N., Calvo, C., & Faggiani, R. (1978). A new investigation of the structure of silver orthophosphate. *Acta Crystallographica Section B Structural Crystallography and Crystal Chemistry*, 34(3), 898–899. <https://doi.org/10.1107/S0567740878014570>
- Nie, L., Duan, B., Lu, A., & Zhang, L. (2019). Pd/TiO₂ @ carbon microspheres derived from chitin for highly efficient photocatalytic degradation of volatile organic compounds. *ACS Sustainable Chemistry & Engineering*, 7(1), 1658–1666. <https://doi.org/10.1021/acssuschemeng.8b05426>
- Nisar, J., Pathak, B., & Ahuja, R. (2012). Screened hybrid density functional study on Sr₂Nb₂O₇ for visible light photocatalysis. *Applied Physics Letters*, 100(18), 181903. <https://doi.org/10.1063/1.4709486>
- Olmo, N. R. S., Saldiva, P. H., do, N., Braga, A. L. F., Lin, C. A., Santos, U., de, P., & Pereirai, L. A. A. (2011). A review of low-level air pollution and adverse effects on human health: Implications for epidemiological studies and public policy. *Clinics (Sao Paulo, Brazil)*, 66(4), 681–690. <https://doi.org/10.1590/s1807-59322011000400025>
- Park, H., Park, Y., Kim, W., & Choi, W. (2013). Surface modification of TiO₂ photocatalyst for environmental applications. *Journal of Photochemistry and Photobiology C: Photochemistry Reviews*, 15, 1–20. <https://doi.org/10.1016/j.jphotochemrev.2012.10.001>

- Passalía, C., Alfano, O. M., & Brandi, R. J. (2017). Integral design methodology of photocatalytic reactors for air pollution remediation. *Molecules*, 22(6), 945–917. <https://doi.org/10.3390/molecules22060945>
- Patil, S. B., Basavarajappa, P. S., Ganganagappa, N., Jyothi, M. S., Raghu, A. V., & Reddy, K. R. (2019). Recent advances in non-metals-doped TiO₂ nanostructured photocatalysts for visible-light driven hydrogen production, CO₂ reduction and air purification. *International Journal of Hydrogen Energy*, 44(26), 13022–13039. <https://doi.org/10.1016/j.ijhydene.2019.03.164>
- Pettit, T., Bettés, M., Chapman, A. R., Hoch, L. M., James, N. D., Irga, P. J., & Torpy, F. R. (2019). The botanical biofiltration of VOCs with active airflow: Is removal efficiency related to chemical properties? *Atmospheric Environment*, 214, 116839. <https://doi.org/10.1016/j.atmosenv.2019.116839>
- Pettit, T., Irga, P. J., & Torpy, F. R. (2018). Towards practical indoor air phytoremediation: A review. *Chemosphere*, 208, 960–974. <https://doi.org/10.1016/j.chemosphere.2018.06.048>
- Pichat, P. (2019). A brief survey of the practicality of using photocatalysis to purify the ambient air (indoors or outdoors) or air effluents. *Applied Catalysis B: Environmental*, 245, 770–776. <https://doi.org/10.1016/j.apcatb.2018.12.027>
- Pirhashemi, M., Habibi-Yangjeh, A., & Rahim Pouran, S. (2018). Review on the criteria anticipated for the fabrication of highly efficient ZnO-based visible-light-driven photocatalysts. *Journal of Industrial and Engineering Chemistry*, 62, 1–25. <https://doi.org/10.1016/j.jiec.2018.01.012>
- Puga, F., Navío, J. A., Jaramillo-Páez, C., Sánchez-Cid, P., & Hidalgo, M. C. (2020). Microwave-assisted sol-gel synthesis of TiO₂ in the presence of halogenhydric acids. Characterization and photocatalytic activity. *Journal of Photochemistry and Photobiology A: Chemistry*, 394, 112457. <https://doi.org/10.1016/j.jphotochem.2020.112457>
- Qadeer, A., Liu, S., Liu, M., Liu, X., Ajmal, Z., Huang, Y., Jing, Y., Khalil, S. K., Zhao, D., Weining, D., Wei, X. Y., & Liu, Y. (2019). Historically linked residues profile of OCPs and PCBs in surface sediments of typical urban river networks, Shanghai: Ecotoxicological state and sources. *Journal of Cleaner Production*, 231, 1070–1078. <https://doi.org/10.1016/j.jclepro.2019.05.203>
- Qadeer, A., Saqib, Z. A., Ajmal, Z., Xing, C., Khan Khalil, S., Usman, M., Huang, Y., Bashir, S., Ahmad, Z., Ahmed, S., Thebo, K. H., & Liu, M. (2020). Concentrations, pollution indices and health risk assessment of heavy metals in road dust from two urbanized cities of Pakistan: Comparing two sampling methods for heavy metals concentration. *Sustainable Cities and Society*, 53, 101959. <https://doi.org/10.1016/j.scs.2019.101959>
- Qiu, W., Dou, K., Zhou, Y., Huang, H., Chen, Y., & Lu, H. (2018). Hierarchical pore structure of activated carbon fabricated by CO₂/microwave for volatile organic compounds adsorption. *Chinese Journal of Chemical Engineering*, 26(1), 81–88. <https://doi.org/10.1016/j.cjche.2017.04.006>
- Rao, X., Dou, H., Long, D., & Zhang, Y. (2020). Ag₃PO₄/g-C₃N₄ nanocomposites for photocatalytic degrading gas phase formaldehyde at continuous flow under 420 nm LED irradiation. *Chemosphere*, 244, 125462. <https://doi.org/10.1016/j.chemosphere.2019.125462>
- Rawal, S. B., Sung, S. D., & Lee, W. I. (2012). Novel Ag₃PO₄/TiO₂ composites for efficient decomposition of gaseous 2-propanol under visible-light irradiation. *Catalysis Communications*, 17, 131–135. <https://doi.org/10.1016/j.catcom.2011.10.034>
- Reyna-Cavazos, K. A., la Cruz, A. M. d., Longoria Rodríguez, F. E., & López-Cuellar, E. (2020). Synthesis of bismuth oxyiodide (BiOI) by means of microwaves in glycerol with

- high photocatalytic activity for the elimination of NO_x and SO₂. *Research on Chemical Intermediates*, 46(1), 923–941. <https://doi.org/10.1007/s11164-019-03998-8>
- Rodriguez Castillo, A. S., Biard, P. F., Guihéneuf, S., Paquin, L., Amrane, A., & Couvert, A. (2019). Assessment of VOC absorption in hydrophobic ionic liquids: Measurement of partition and diffusion coefficients and simulation of a packed column. *Chemical Engineering Journal and the Biochemical Engineering Journal*, 360, 1416–1426. <https://doi.org/10.1016/j.cej.2018.10.146>
- Ferraa, S., Naciri, Y., Hsini, A., Barebita, H., Bouziani, A., Albourine, A., Nimour, A., & Guedira, T. (2021). Evolution of the physicochemical and photocatalytic properties of BaO embedded in bismuth phosphovanadates glasses. *Chemical Physics Letters*, 763, 138173. <https://doi.org/10.1016/j.cplett.2020.138173>
- Saadetnejad, D., & Yıldırım, R. (2018). Photocatalytic hydrogen production by water splitting over Au/Al-SrTiO₃. *International Journal of Hydrogen Energy*, 43(2), 1116–1122. <https://doi.org/10.1016/j.ijhydene.2017.10.154>
- Sansotera, M., Geran Malek Kheyli, S., Baggioli, A., Bianchi, C. L., Pedferri, M. P., Diamanti, M. V., & Navarrini, W. (2019). Absorption and photocatalytic degradation of VOCs by perfluorinated ionomeric coating with TiO₂ nanopowders for air purification. *Chemical Engineering Journal and the Biochemical Engineering Journal*, 361, 885–896. <https://doi.org/10.1016/j.cej.2018.12.136>
- Schneider, J., Matsuoka, M., Takeuchi, M., Zhang, J., Horiuchi, Y., Anpo, M., & Bahnemann, D. W. (2014). Understanding TiO₂ photocatalysis: mechanisms and materials. *Chemical Reviews*, 114(19), 9919–9986. <https://doi.org/10.1021/cr5001892>
- Shaim, A., Amaterz, E., Naciri, Y., Taoufyq, A., Bakiz, B., Ezahri, M., Benlhachemi, A., Ouammou, A., & Chahine, A. (2019). Synthesis, characterization and photocatalytic activity of titanophosphate glasses. *Mediterranean Journal of Chemistry*, 8(1), 66–73. <https://doi.org/10.13171/mjc8119032221as>
- Shammy, A., Sivret, E. C., Le-Minh, N., Lebrero Fernandez, R., Evanson, I., & Stuetz, R. M. (2016). Review of odour abatement in sewer networks. *Journal of Environmental Chemical Engineering*, 4(4), 3866–3881. <https://doi.org/10.1016/j.jece.2016.08.016>
- Shayegan, Z., Haghghat, F., & Lee, C. S. (2020). Carbon-doped TiO₂ film to enhance visible and UV light photocatalytic degradation of indoor environment volatile organic compounds. *Journal of Environmental Chemical Engineering*, 8(5), 104162. <https://doi.org/10.1016/j.jece.2020.104162>
- Shayegan, Z., Lee, C. S., & Haghghat, F. (2018). TiO₂ photocatalyst for removal of volatile organic compounds in gas phase – A review. *Chemical Engineering Journal and the Biochemical Engineering Journal*, 334, 2408–2439. <https://doi.org/10.1016/j.cej.2017.09.153>
- Shen, Y., Zhu, Z., Wang, X., Khan, A., Gong, J., & Zhang, Y. (2018). Synthesis of Z-scheme g-C₃N₄/Ag/Ag₃PO₄ composite for enhanced photocatalytic degradation of phenol and selective oxidation of gaseous isopropanol. *Materials Research Bulletin*, 107, 407–415. <https://doi.org/10.1016/j.materresbull.2018.08.017>
- Sleiman, M., Conchon, P., Ferronato, C., & Chovelon, J. M. (2009). Photocatalytic oxidation of toluene at indoor air levels (ppbv): Towards a better assessment of conversion, reaction intermediates and mineralization. *Applied Catalysis B: Environmental*, 86(3–4), 159–165. <https://doi.org/10.1016/j.apcatb.2008.08.003>
- Sui, H., An, P., Li, X., Cong, S., & He, L. (2017). Removal and recovery of o-xylene by silica gel using vacuum swing adsorption. *Chemical Engineering Journal and the Biochemical Engineering Journal*, 316, 232–242. <https://doi.org/10.1016/j.cej.2017.01.061>

- Suresh, S., & Bandosz, T. J. (2018). Removal of formaldehyde on carbon -based materials: A review of the recent approaches and findings. *Carbon N Carbon*, 137, 207–221. <https://doi.org/10.1016/j.carbon.2018.05.023>
- Swetha, G., Gopi, T., Chandra Shekar, S., Ramakrishna, C., Saini, B., & Rao, P. V. L. (2017). Combination of adsorption followed by ozone oxidation with pressure swing adsorption technology for the removal of VOCs from contaminated air streams. *Chemical Engineering Research and Design*, 117, 725–732. <https://doi.org/10.1016/j.cherd.2016.11.036>
- Tang, M., Ao, Y., Wang, C., & Wang, P. (2020). Facile synthesis of dual Z-scheme g-C₃N₄/Ag₃PO₄/AgI composite photocatalysts with enhanced performance for the degradation of a typical neonicotinoid pesticide. *Applied Catalysis B: Environmental*, 268, 118395. <https://doi.org/10.1016/j.apcatb.2019.118395>
- Taranto, J., Frochot, D., & Pichat, P. (2009). Photocatalytic air purification: Comparative efficacy and pressure drop of a TiO₂-coated thin mesh and a honeycomb monolith at high air velocities using a 0.4 m³ close-loop reactor. *Separation and Purification Technology*, 67(2), 187–193. <https://doi.org/10.1016/j.seppur.2009.03.017>
- Thevenet, F., Sivachandiran, L., Guaitella, O., Barakat, C., & Rousseau, A. (2014). Plasma-catalyst coupling for volatile organic compound removal and indoor air treatment: A review. *Journal of Physics D: Applied Physics*, 47(22), 224011. <https://doi.org/10.1088/0022-3727/47/22/224011>
- Tian, N., Zhang, Y., Li, X., Xiao, K., Du, X., Dong, F., Waterhouse, G. I. N., Zhang, T., & Huang, H. (2017). Precursor-reforming protocol to 3D mesoporous g-C₃N₄ established by ultrathin self-doped nanosheets for superior hydrogen evolution. *Nano Energy*, 38, 72–81. <https://doi.org/10.1016/j.nanoen.2017.05.038>
- Wan, S., Ou, M., Zhong, Q., & Zhang, S. (2018). Z-scheme CaIn₂S₄/Ag₃PO₄ nanocomposite with superior photocatalytic NO removal performance: Fabrication, characterization and mechanistic study. *New Journal of Chemistry*, 42(1), 318–326. <https://doi.org/10.1039/C7NJ03588H>
- Wang, K., Liu, C., Du, P., Zheng, J., & Gong, X. (2015). Bulk heterojunction perovskite hybrid solar cells with large fill factor. *Energy & Environmental Science*, 8(4), 1245–1255. <https://doi.org/10.1039/C5EE00222B>
- Wang, X., Yu, J., Fu, C., Li, T., & Yu, H. (2019). Self-templated formation of AgCl/TiO₂ hollow octahedra for improved visible-light photocatalytic activity. *Applied Surface Science*, 494, 740–748. <https://doi.org/10.1016/j.apsusc.2019.07.221>
- Wen, X. J., Shen, C. H., Fei, Z. H., Fang, D., Liu, Z. T., Dai, J. T., & Niu, C. G. (2020). Recent developments on AgI based heterojunction photocatalytic systems in photocatalytic application. *Chemical Engineering Journal and the Biochemical Engineering Journal*, 383, 123083. <https://doi.org/10.1016/j.cej.2019.123083>
- Wood, P. M. (1988). The potential diagram for oxygen at pH 7. *The Biochemical Journal*, 253(1), 287–289. <https://doi.org/10.1042/bj2530287>
- Xian, S., Yu, Y., Xiao, J., Zhang, Z., Xia, Q., Wang, H., & Li, Z. (2015). Competitive adsorption of water vapor with VOCs dichloroethane, ethyl acetate and benzene on MIL-101(Cr) in humid atmosphere. *RSC Advances*, 5(3), 1827–1834. <https://doi.org/10.1039/C4RA10463C>
- Xiao, G., Wang, X., Li, D., & Fu, X. (2008). InVO₄-sensitized TiO₂ photocatalysts for efficient air purification with visible light. *Journal of Photochemistry and Photobiology A: Chemistry*, 193(2-3), 213–221. <https://doi.org/10.1016/j.jphotochem.2007.06.027>
- Xie, J., Yang, Y., He, H., Cheng, D., Mao, M., Jiang, Q., Song, L., & Xiong, J. (2015). Facile synthesis of hierarchical Ag₃PO₄/TiO₂ nanofiber heterostructures with highly enhanced

- visible light photocatalytic properties. *Applied Surface Science*, 355, 921–929. <https://doi.org/10.1016/j.apsusc.2015.07.175>
- Xin, X., Li, S. H., Zhang, N., Tang, Z. R., & Xu, Y. J. (2019). 3D graphene/AgBr/Ag cascade aerogel for efficient photocatalytic disinfection. *Applied Catalysis B: Environmental*, 245, 343–350. <https://doi.org/10.1016/j.apcatb.2018.12.066>
- Xu, L., Huang, W. Q., Wang, L. L., Huang, G. F., & Peng, P. (2014). Mechanism of superior visible-light photocatalytic activity and stability of hybrid Ag_3PO_4 /graphene nanocomposite. *The Journal of Physical Chemistry C*, 118(24), 12972–12979. <https://doi.org/10.1021/jp5034273>
- Xue, W., Huang, D., Wen, X., Chen, S., Cheng, M., Deng, R., Li, B., Yang, Y., & Liu, X. (2020). Silver-based semiconductor Z-scheme photocatalytic systems for environmental purification. *Journal of Hazardous Materials*, 390, 122128 <https://doi.org/10.1016/j.jhazmat.2020.122128>
- Yang, H., Tian, J., Bo, Y., Zhou, Y., Wang, X., & Cui, H. (2017). Visible photocatalytic and photoelectrochemical activities of TiO_2 nanobelts modified by In_2O_3 nanoparticles. *Journal of Colloid and Interface Science*, 487, 258–265. <https://doi.org/10.1016/j.jcis.2016.10.051>
- Yang, S. B., Chun, H. H., Tayade, R. J., & Jo, W. K. (2015). Iron-functionalized titanium dioxide on flexible glass fibers for photocatalysis of benzene, toluene, ethylbenzene, and o-xylene (BTEX) under visible- or ultraviolet-light irradiation. *Journal of the Air & Waste Management Association (1995)*, 65(3), 365–373. <https://doi.org/10.1080/10962247.2014.995838>
- Yi, Z., Ye, J., Kikugawa, N., Kako, T., Ouyang, S., Stuart-Williams, H., Yang, H., Cao, J., Luo, W., Li, Z., Liu, Y., & Withers, R. L. (2010). An orthophosphate semiconductor with photooxidation properties under visible-light irradiation. *Nature Materials*, 9(7), 559–564. <https://doi.org/10.1038/nmat2780>
- Yue, X., Yi, S., Wang, R., Zhang, Z., & Qiu, S. (2018). Well-controlled SrTiO_3 @ Mo_2C core-shell nanofiber photocatalyst: Boosted photo-generated charge carriers transportation and enhanced catalytic performance for water reduction. *Nano Energy*, 47, 463–473. <https://doi.org/10.1016/j.nanoen.2018.03.014>
- Zazueta, A. L. L., Destailhats, H., & Li Puma, G. (2013). Radiation field modeling and optimization of a compact and modular multi-plate photocatalytic reactor (MPPR) for air/water purification by Monte Carlo method. *Chemical Engineering Journal and the Biochemical Engineering Journal*, 217, 475–485. <https://doi.org/10.1016/j.cej.2012.11.085>
- Zhang, J., Bang, J. H., Tang, C., & Kamat, P. V. (2010). Tailored TiO_2 - SrTiO_3 heterostructure nanotube arrays for improved photoelectrochemical performance. *ACS Nano*, 4(1), 387–395. <https://doi.org/10.1021/nn901087c>
- Zhang, N., Nguyen, A. V., & Zhou, C. (2018). A review of the surface features and properties, surfactant adsorption and floatability of four key minerals of diasporic bauxite resources. *Advances in Colloid and Interface Science*, 254, 56–75. <https://doi.org/10.1016/j.jcis.2018.03.005>
- Zhang, X., Gao, B., Creamer, A. E., Cao, C., & Li, Y. (2017). Adsorption of VOCs onto engineered carbon materials: A review. *Journal of Hazardous Materials*, 338, 102–123. <https://doi.org/10.1016/j.jhazmat.2017.05.013>
- Zhao, F. M., Pan, L., Wang, S., Deng, Q., Zou, J. J., Wang, L., & Zhang, X. (2014). $\text{Ag}_3\text{PO}_4/\text{TiO}_2$ composite for efficient photodegradation of organic pollutants under visible light. *Applied Surface Science*, 317, 833–838. <https://doi.org/10.1016/j.apsusc.2014.09.022>

- Zhao, J., & Yang, X. (2003). Photocatalytic oxidation for indoor air purification: A literature review. *Building and Environment*, 38(5), 645–654. [https://doi.org/10.1016/S0360-1323\(02\)00212-3](https://doi.org/10.1016/S0360-1323(02)00212-3)
- Zhao, Z., Fan, J., Liu, W., Xue, Y., & Yin, S. (2017). In-situ hydrothermal synthesis of $\text{Ag}_3\text{PO}_4/\text{g-C}_3\text{N}_4$ composite and their photocatalytic decomposition of NO_x . *Journal of Alloys and Compounds*, 695, 2812–2819. <https://doi.org/10.1016/j.jallcom.2016.12.001>
- Zhong, L., Haghghat, F., & Lee, C. S. (2013). Ultraviolet photocatalytic oxidation for indoor environment applications: Experimental validation of the model. *Building and Environment*, 62, 155–166. <https://doi.org/10.1016/j.buildenv.2013.01.009>
- Zhou, H., Wen, Z., Liu, J., Ke, J., Duan, X., & Wang, S. (2019). Z-scheme plasmonic Ag decorated $\text{WO}_3/\text{Bi}_2\text{WO}_6$ hybrids for enhanced photocatalytic abatement of chlorinated-VOCs under solar light irradiation. *Applied Catalysis B: Environmental*, 242, 76–84. <https://doi.org/10.1016/j.apcatb.2018.09.090>
- Zhou, P., Yu, J., & Jaroniec, M. (2014). All-solid-state Z-scheme photocatalytic systems. *Advanced Materials (Deerfield Beach, Fla.)*, 26(29), 4920–4935. <https://doi.org/10.1002/adma.201400288>
- Zhu, L., Shen, D., & Luo, K. H. (2020). A critical review on VOCs adsorption by different porous materials: Species, mechanisms and modification methods. *Journal of Hazardous Materials*, 389, 122102. <https://doi.org/10.1016/j.jhazmat.2020.122102>
- Zouzelka, R., & Rathousky, J. (2017). Photocatalytic abatement of NO_x pollutants in the air using commercial functional coating with porous morphology. *Applied Catalysis B: Environmental*, 217, 466–476. <https://doi.org/10.1016/j.apcatb.2017.06.009>